Atmospheric Research 122 (2013) 520–543

Contents lists available at SciVerse ScienceDirect

Atmospheric Research

journal homepage: www.elsevier.com/locate/atmos

Characterizing the vertical profile of aerosol particle extinction and linear depolarization over Southeast Asia and the Maritime Continent: The 2007–2009 view from CALIOP

James R. Campbell [a,*], Jeffrey S. Reid [a], Douglas L. Westphal [a], Jianglong Zhang [b], Jason L. Tackett [c], Boon Ning Chew [d], Ellsworth J. Welton [e], Atsushi Shimizu [f], Nobuo Sugimoto [f], Kazuma Aoki [g], David M. Winker [h]

[a] Aerosol and Radiation Sciences Section, Marine Meteorology Division, Naval Research Laboratory, Monterey, CA, USA
[b] Department of Atmospheric Sciences, University of North Dakota, Grand Folks, ND, USA
[c] Science Systems and Applications Inc., c/o NASA Langley Research Center, Hampton, VA, USA
[d] Center for Remote Imaging, Sensing and Processing, National University of Singapore, Singapore
[e] NASA Goddard Space Flight Center, Greenbelt, MD, USA
[f] National Institute for Environmental Studies, Tsukuba, Japan
[g] Department of Earth Sciences, University of Toyama, Toyama, Japan
[h] NASA Langley Research Center, Hampton, VA, USA

ARTICLE INFO

Article history:
Received 5 August 2011
Received in revised form 6 March 2012
Accepted 12 May 2012

Keywords:
CALIPSO
Lidar
Southeast Asia
Maritime Continent
Aerosol particle scattering
Aerosol composition

ABSTRACT

Vertical profiles of 0.532 μm aerosol particle extinction coefficient and linear volume depolarization ratio are described for Southeast Asia and the Maritime Continent. Quality-screened and cloud-cleared Version 3.01 Level 2 NASA Cloud Aerosol Lidar with Orthogonal Polarization (CALIOP) 5-km Aerosol Profile datasets are analyzed from 2007 to 2009. Numerical simulations from the U.S. Naval Aerosol Analysis and Predictive System (NAAPS), featuring two-dimensional variational assimilation of NASA Moderate Resolution Imaging Spectroradiometer and Multi-angle Imaging Spectro-Radiometer quality-assured datasets, combined with regional ground-based lidar measurements, are considered for assessing CALIOP retrieval performance, identifying bias, and evaluating regional representativeness. CALIOP retrievals of aerosol particle extinction coefficient and aerosol optical depth (AOD) are high over land and low over open waters relative to NAAPS (0.412/0.312 over land for all data points inclusive, 0.310/0.235 when the per bin average is used and each is treated as single data points; 0.102/0.151 and 0.086/0.124, respectively, over ocean). Regional means, however, are very similar (0.180/0.193 for all data points and 0.155/0.159 when averaged per normalized bin), as the two factors offset one another. The land/ocean offset is investigated, and discrepancies attributed to interpretation of particle composition and a-priori assignment of the extinction-to-backscatter ratio ("lidar ratio") necessary for retrieving the extinction coefficient from CALIOP signals. Over land, NAAPS indicates more dust present than CALIOP algorithms are identifying, indicating a likely assignment of a higher lidar ratio representative of more absorptive particles. NAAPS resolves more smoke over water than identified with CALIOP, indicating likely usage of a lidar ratio characteristic of less absorptive particles to be applied that biases low AOD there. Over open waters except within the Bay of Bengal, aerosol particle scattering is largely capped below 1.5 km MSL, though ground-based lidar measurements at Singapore differ slightly from this finding. Significant aerosol particle presence over land is similarly capped near 3.0 km MSL over most regions. Particle presence at low levels regionally, except over India, is dominated by relatively non-depolarizing particles. Industrial haze, sea salt droplets and fresh smoke are thus most likely present.

Published by Elsevier B.V.

* Corresponding author. Tel.: +1 8316564555; fax: +1 8316564769.
E-mail address: james.campbell@nrlmry.navy.mil (J.R. Campbell).

0169-8095/$ – see front matter. Published by Elsevier B.V.
doi:10.1016/j.atmosres.2012.05.007

1. Introduction

1.1. The role of satellite-based lidar in observing the aerosol system of Southeast Asia and the Maritime Continent

With the proliferation of satellite-based atmospheric remote sensors used for applied research (e.g., King et al., 1999), embodied notably through the suite of instruments supported by the National Aeronautics and Space Administration Earth Observing System (NASA EOS) program (Chuvieco and Justice, 2008), understanding of the role that aerosol particles play in the planetary radiation budget has improved (IPCC, 2007). Of all significant anthropogenic atmospheric components contributing to global radiative equilibrium, however, uncertainties regarding aerosol particle presence and microphysical variability remain highest (Schwartz and Andreae, 1996; Rotstayn and Penner, 2001; Anderson et al., 2003a; IPCC, 2007). Inadequate characterization of aerosol optical properties has a far-reaching consequence. Numerical models incapable of resolving significant aerosol particle presence and/or their microphysical characteristics may accurately constrain surface and top-of-the-atmosphere radiative fluxes, particularly as such measurements are increasingly available and model assimilation schemes are maturing (Loeb et al., 2003; Loeb et al., 2009). They do so, however, at the risk of inaccurately deriving column heating/cooling rates, and thus thermodynamic structure, which can significantly degrade skill for depicting regional circulation and oscillatory regimes governing climate (Lau et al., 2008; Tian et al., 2008; Luo et al., 2009; Kuhlmann and Quass, 2010).

Whereas many passive-based satellite instruments measure scattered visible and near-infrared atmospheric radiances, which are devolved into column-integrated aerosol particle optical and microphysical properties like aerosol optical depth (AOD) and fine/course mode partitioning fractions (e.g., Tanré et al., 1997; Kaufman et al., 1997a; Martonchik et al., 1997), these instruments are limited at best from collecting vertically-resolved information. In response, NASA in collaboration with the French Centre National d'Études Spatiales (CNES), developed the three-channel Cloud Aerosol Lidar with Orthogonal Polarization instrument (0.532 μm with linear polarization diversity, and 1.064 μm; CALIOP) flown aboard the EOS Cloud–Aerosol Lidar and Infrared Pathfinder Satellite Observation (CALIPSO) satellite (Winker et al., 2009). Lidar instruments are uniquely tuned to the detection of aerosol particle and optically-thin hydrometeor cloud scattering, and collect range-resolved information with relatively high vertical resolution (~1–100 m; Measures, 1984). Sensitivity to the linear polarization plane of backscatter signal provides ancillary information for helping characterize aerosol particle type, composition and likely surface source (Sassen, 2000; Liu et al., 2009). With global coverage, diurnal profiling capabilities, and set within the EOS "A-Train" constellation of complimentary passive and active remote sensors (Stephens et al., 2002), thus contributing to an unmatched synergy for joint cloud and aerosol observation, CALIOP profiling has revolutionized global aerosol particle research (Winker et al., 2006, 2010).

Perhaps in no other climate regime is the necessity for comprehensive satellite observation of aerosol particles more critical than that of Southeast Asia (SA) and the nearby islands and waters of the Maritime Continent (MC). Reid et al. (2012) and Reid et al. (2013–this issue), considered in context with Reid et al. (2012), establish the present state of understanding for annual and inter-seasonal SA/MC aerosol particle two-dimensional (x, y; 2D) distributions, corresponding surface source activity, including the influence of regional biomass burning and its covariance with synoptic climate, and the efficacy of satellite-based algorithms designed for retrieving aerosol particle optical properties. They describe the SA/MC aerosol system as a unique confluence of urban and industrial anthropogenic sources, domestic, agricultural and natural burning of regional grasslands, deltas, savannahs and forests, with subsequent chemical processing over the salt-rich marine waters. The region is further subject to transport of aeolian dusts from the north-central sub-continent and even Sahara (e.g., Lee et al., 2006). In spite of a reasonably stable tropical climate, SA/MC aerosol particle composition and microphysical variability are highly complex.

Reid et al. (2012) and Reid et al. (2013–this issue) further explain why SA/MC aerosol particle physical properties are critically under-constrained for parameterization in radiative/climate models. From an observability standpoint, isolating the aerosol particle signal in SA/MC satellite datasets is daunting. Marine layer cumulus and stratocumulus clouds, widespread convective activity with cumulonimbus cloud towers and ice-crystal anvil outflow (e.g., Kang et al., 1999), and the close proximity of the tropical western Pacific warm pool and subsequent tropical tropopause transition layer, where optically-thin cirrus clouds propagate with increasing persistence toward the regional southeast (McFarquhar et al., 2000; Gettelman and Forster, 2002; Riihimaki and McFarlane, 2010; Virts and Wallace, 2010), all combine to create a viewing scene from space that is regularly cloud-contaminated (Hsu et al., 2003). With limited surface infrastructure, and thus a limited distribution of ground-based observing sites, the challenges of characterizing the SA/MC aerosol system are considerable.

Overcoming system observability challenges through coordinated ground/satellite remote sensing and the compilation of regionally representative datasets for climate study are the founding basis for the Seven Southeast Asian Studies (7SEAS) program (http://7-seas.gsfc.nasa.gov; http://www.nrlmry.navy.mil/flambe/7seas/7seas.html). These efforts are compulsory if the community is to resolve outstanding regional issues related to direct, semi-direct and indirect aerosol particle forcing. As such, this paper describes the critical third dimension for SA/MC aerosol particle presence, composition, and optical scattering efficiency. Vertical profiles of aerosol particle extinction and linear depolarization are described for a three-year cloud-cleared and quality-assured CALIOP data subset (2007–2009). Annual and seasonal mean AOD and particle composition are evaluated for representativeness versus a global forecast model equipped with 2D variational (2DVAR; x, y) assimilation of quality-screened AOD datasets collected by NASA Moderate Resolution Imaging Spectroradiometer instrument (MODIS; King et al., 1992) from both the Terra and Aqua satellites, and Multi-angle Imaging SpectroRadiometer instrument (MISR; Diner et al., 1998). Annual and seasonal mean aerosol particle extinction coefficients and linear volume depolarization ratio (LVDR), solved on a $1^\circ \times 1^\circ$ regional grid, are reported at five levels above mean sea level (MSL) and investigated for magnitude and variability, and interpreted for predominant composition and likely corresponding surface source. The

analysis is refined for detailed quantitative comparison between CALIOP and the model within seven SA/MC sub-sectors. CALIOP-derived extinction coefficient profiles are compared with ground-based lidar observations in two sub-sectors. The fractional contribution to total extinction for each of six discrete CALIOP aerosol models used in constraining algorithm retrievals are investigated for regional representativeness. The result is a comprehensive three-year study of the physical attributes of SA/MC aerosol particles, as actively profiled from space.

2. CALIOP Level 2 aerosol profile datasets: a 2007–2009 subset, screening protocols, data averaging, and regional representativeness

2.1. CALIOP Level 2 aerosol particle profiles and quality-assurance screening

Version 3.01 CALIOP Level 2 aerosol profile products (L2-AProf) include 0.532 μm extinction coefficients and LVDR profiles derived in 5-km along-track segments at 60 m vertical resolution and separated into contiguous daytime and nighttime granule files. Retrievals for extinction coefficient from CALIOP signal profiles are indirect. That is, since CALIOP is an elastic-backscatter lidar instrument, the equation for lidar scattering contains two distinct unknown terms: particulate extinction and backscatter coefficients, where corresponding molecular terms are estimated based on thermal density profiles derived from a global climate model (Winker et al., 2009).

CALIOP aerosol particle optical retrievals are conducted using the Hybrid Extinction Retrieval Algorithm package (Young and Vaughan, 2009), which is predicated on a-priori assignment of a multiple-scattering correction factor (nominally set to unity for aerosol particles) and the ratio for extinction and backscatter coefficients (Omar et al., 2009). The latter term, the so-called "lidar ratio" is assumed constant vertically within identified layers (Liu et al., 2009; Omar et al., 2009), and is necessary for constraining the lidar equation and solving extinction and backscatter (Young and Vaughan, 2009; Oo and Holz, 2011). Retrieval uncertainties are propagated through each step of the solution beginning from an estimate of the signal noise scale factor solved at each range bin reported in the Level 1B attenuated backscatter product at 20.16 Hz pulse repetition frequency and 30/60 m vertical resolutions, for 0.0 to 8.2 and 8.2 to 20.1 km MSL, respectively (Liu et al., 2006). Only data from 0.0 to 10.0 km MSL are considered in this analysis. Uncertainties induced by a-priori assignment of the lidar ratio are parameterized at between 30 and 50%, depending on aerosol model, and thus propagated through each bin-relative solution for extinction.

L2-AProf datasets are pre-processed for this study in two steps. Profiles are screened if aerosol particles are not present within 250 m of the surface or if cloud is observed anywhere within the column of the 5-km along-track sample average. For SA/MC, this is a rigid requirement, given the frequency of high aerosol optical depth events (e.g., Remer et al., 2008; Reid et al., 2012a) and widespread cloud occurrence. However, lidar instruments are subject to complete source pulse attenuation at visible optical depths approaching 3.0 (Sassen and Cho, 1992). With CALIOP, and given persistently high regional background rates (i.e., noise) from the direct scattering of visible solar light at high zenith angles during daytime overpasses, this threshold can effectively be lowered (Hunt et al., 2009; Vaughan et al., 2009). Requirement of aerosol scattering within 250 m of the ground alleviates concern for attenuation-limited cases biasing the subset, as well as simple undersampling of layers nearest the surface that impact the overall mean. Additionally, cloud scattering above an aerosol layer causes transmission losses, which if not properly corrected will cause error propagation within the iterated solution for extinction coefficient and, subsequently, AOD.

After profile screening, a filtering scheme is next applied to the 60 m bins in each qualifying 5-km profile that isolates quality-assured (QA) aerosol particle information. Based on parameter profiles included in L2-AProf, and described elsewhere (NASA, 2010), a 60-m extinction coefficient, and consequently corresponding LVDR, are included within a QA profile if

(1) Extinction_QC_532(r) is equal to 0, 1, 2, 16 or 18,
(2) $-20 \geq$ CAD_Score(r) ≥ -100,
(3) Extinction_Coefficient_Uncertainty_532(r) $\leq 10\ \mathrm{km}^{-1}$,
(4) Atmospheric_Volume_Description(r^*, bits 1–3) is equal to 3, and
(5) Atmospheric_Volume_Description(r^*, bits 10–12) is not equal to 0,

where (r) relates each value as a function of range. Tackett et al. (in preparation) describe a similar rubric for generating what they term "Level 3" CALIOP aerosol profile datasets. Differences between the two are slight, as described further by Campbell et al. (2012).

Extinction_QC_532 relates to the application of the a-priori lidar ratio, and whether or not the solution for extinction coefficient and column-integrated AOD converge (i.e., solution is stable) or diverge (i.e., solution becomes unstable). CALIOP aerosol retrievals make use of six discrete models representing typical aerosol mixtures (clean marine, dust, polluted continental, clean continental, polluted dust and smoke). A characteristic lidar ratio for each type has been determined from observations. An algorithm, making use of observed CALIOP signals, then attempts to identify the appropriate aerosol model (Omar et al., 2009). The lidar ratio associated with the model is then used in the extinction retrieval. If the prescribed lidar ratio is wildly in error, the solution will diverge causing the algorithm to adjust the a-priori value, reiterate and reevaluate. If a stable result is not then achieved, or if the solution does not fall within a range of acceptable values for AOD and/or magnitudes of extinction, as signified by one of the five values for this flag noted above, these cases are conservatively removed.

CAD_Score relates to the classification of aerosol particle presence, as opposed to cloud, to within a relative degree of confidence. Extinction_Coefficient_Uncertainty values set to 99 km^{-1} reflect an unstable retrieval. Again conservatively, a threshold of 10 km^{-1} is applied. Atmospheric_Volume_Description at bits 1–3 describes the type of particle identified, whereby '3' indicates aerosol. At bits 10–12, it denotes one of eight types of aerosol particles identified. Each of the six models introduced above are included, as are cases of 'other' and 'not determined', the latter of which are rejected. A profile with no aerosol particle extinction solved (i.e., AOD = 0) is presumed to be the result of compromised instrument detection limits and is removed.

Data are reported in L2-AProf at 60 m vertical resolution. Therefore, measurements below 8.2 km MSL reflect two-bin averages of raw 30 m resolution Level 1B data. However, consecutive 30 m bins representing either cloud or aerosol scattering are never averaged together to yield a single 60 m bin in L2-AProf, since cloud and aerosol extinction are always reported separately [Vaughan, M. A. 2011, personal communication]. For (4) and (5), r^* thus relates to the possibility that one of the two bins representing the average reported by Atmospheric_Volume_Description may not equal 3 (i.e., does not represent aerosol scattering), though the other must. Since such a bin cannot represent cloud, and is instead either 'Clear Air', or 'Surface Return', and neither extinction coefficient nor LVDR are reported for these latter two bin types, we include these 60 m data points in the analysis, for they reflect the corresponding aerosol-related value. Furthermore, LVDR are only considered in the analysis for bins identified as representing aerosol particles, thus avoiding aliasing by near-zero values (nominally 1.4%) induced by clear air (e.g., Bridge and Buckingham, 1966).

Annual and seasonal mean CALIOP profiles of aerosol particle extinction coefficient and LVDR are derived on a $1^\circ \times 1^\circ$ regional horizontal grid at 100 m vertical resolution. This grid corresponds with that of a global aerosol transport model, considered in Section 2b for comparison and evaluation. Campbell et al. (2010) describe the use of a Hanning function for constructing CALIOP data averages coinciding within a single model grid box, applied here for generating mean grid-resolved profiles of mean extinction and LVDR, such that data points collected further away from its center are weighted less than the closer ones. The center of the 5-km along-track CALIOP average is used as the horizontal reference point relative to the model grid center. Spatial half-widths of 150 m vertically, and a horizontal length equal to the distance of the grid point center to the respective corner of its equatorward $1^\circ \times 1^\circ$ bin extent are used.

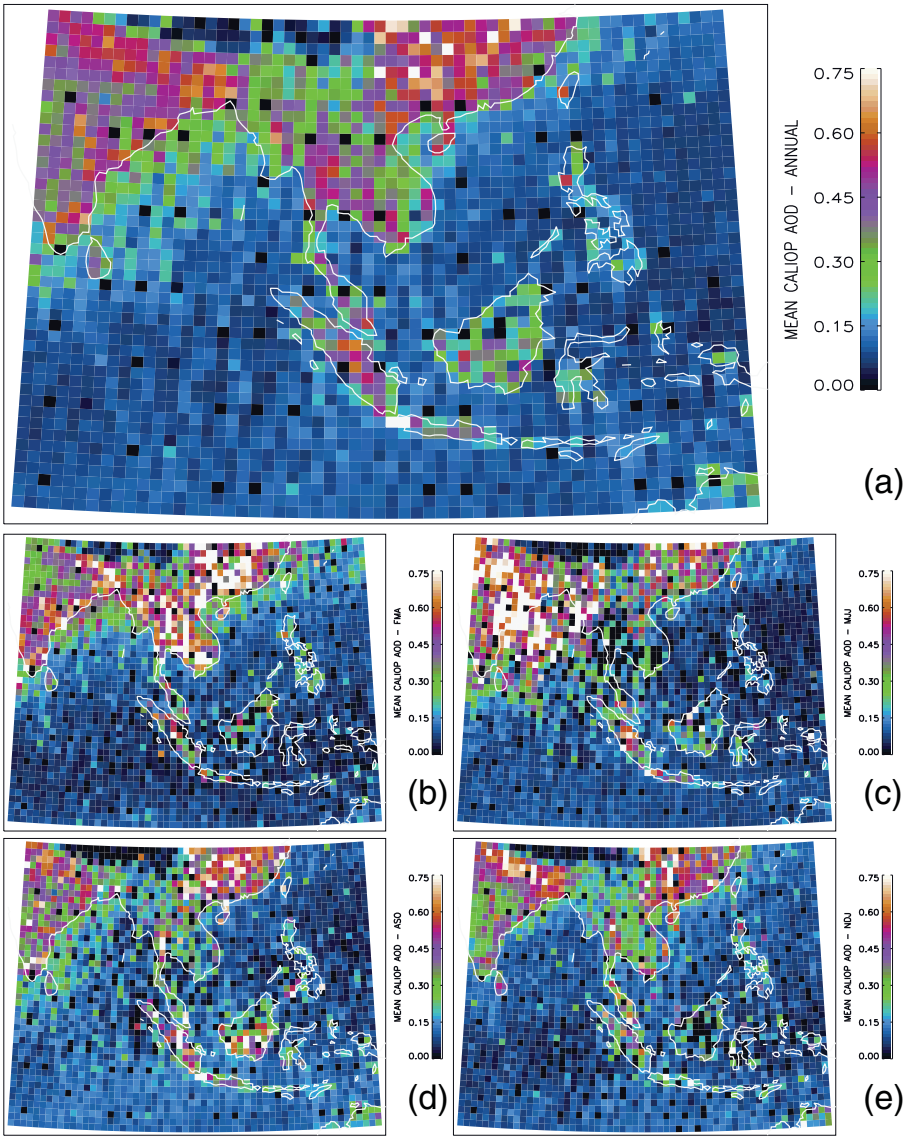

Fig. 1. For 2007–2009 at $1^\circ \times 1^\circ$ resolution, (a) mean annual CALIOP 0.532 μm AOD over the Southeast Asia/Maritime Continent (SA/MC) domain for quality-assured cloud-cleared retrievals, and corresponding three-month seasonal composites for (b) February, March, April (FAM), (c) May, June, July (MJJ), (d) August, September, October (ASO) and (e) November, December, January (NDJ).

2.2. Evaluating the representativeness of CALIOP retrievals in SA/MC

Understanding how well CALIOP-derived aerosol particle optical retrievals represent the SA/MC system is next investigated versus a regional reference dataset. The *U.S. Navy Aerosol Analysis and Prediction System* (NAAPS) is a 1°×1° global aerosol mass transport model that computes 6-day forecasts of smoke, dust, sulfate, sea salt and SO_2 mass concentration every 6 h. NAAPS data are generated using a version of the *Navy Atmospheric Variational Data Assimilation System* (NAVDAS) *for Aerosol Optical Depth* [NAVDAS-AOD; Zhang et al., 2005; Zhang and Reid, 2006, 2009] that conducts 2DVAR assimilation of quality-screened MODIS over-ocean (Zhang and Reid, 2006; Shi et al., 2011a) and over-land AOD products (Hyer et al., 2011), and Version 1 of an assimilation-grade MISR AOD product (Shi, 2009). Descriptions of NAVDAS-AOD and its impact on NAAPS performance are described by Zhang et al. (2008) and Reid et al. (2009). With 2DVAR assimilation, NAAPS 00-h skill is comparable with that of satellite retrievals (e.g., Zhang et al., 2008; Zhang and Reid, 2010; Hyer et al., 2011). Forecasts improve by 20–40% (Zhang et al., 2008; Zhang et al., 2011).

NAAPS 0.550 μm AOD corresponding with CALIOP retrievals at the closest model grid point in time and space are compiled and assessed for corresponding annual and inter-seasonal means. Though as many as 3 h and roughly 50 km (depending on latitude) offset can occur between a CALIOP retrieval and the closest model analysis, this is reasonable compared with covariance metrics described by Anderson et al. (2003b) and Zhang et al. (2008) for aerosol physical properties, as these settings exceed 0.8 for autocorrelation both temporally and spatially.

Since both day and nighttime CALIOP retrievals are used in this analysis, comparison with corresponding NAAPS data is somewhat indirect, even putting aside the slight difference in wavelength (3% for an Angstrom Exponent of 1.0). As described by Campbell et al. (2012), nighttime NAAPS AODs

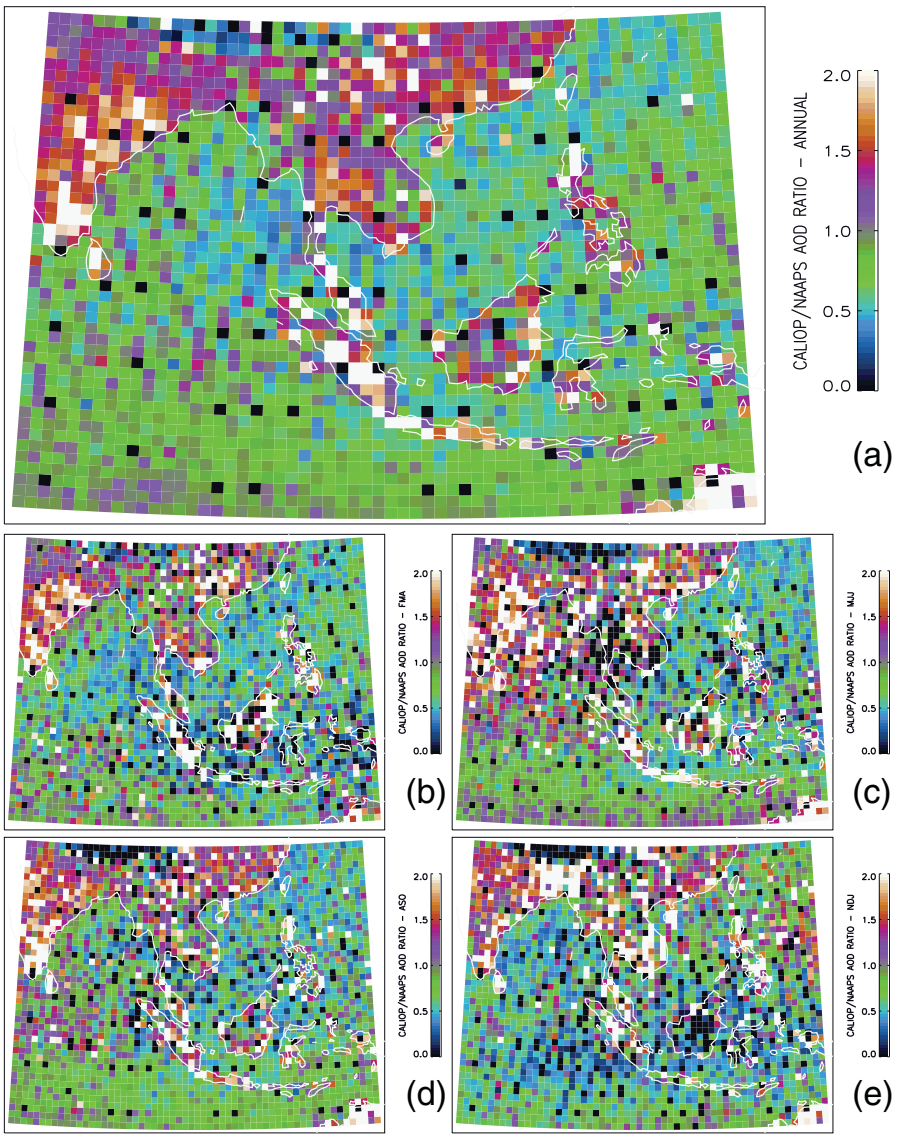

Fig. 2. For 2007–2009 at 1°×1° resolution, (a) mean annual ratio of CALIOP 0.532 μm AOD versus NAAPS 0.550 μm AOD for the SA/MC domain for corresponding quality-assured cloud-cleared retrievals, and three-month seasonal composites for (b) FAM, (c) MJJ, (d) ASO and (e) NDJ.

represent a 12-h forecast, at best, from lack of MODIS and/or MISR data for assimilation in the dark sector of the model as it is initialized. NAAPS 00-h AOD analysis skill is consistent with that exhibited by both MODIS and MISR, which is logical since these data are assimilated. However, performance degradation occurs through the model forecast cycle, which must be quantified in order to establish a credible comparison. This issue is discussed further in Appendix A, referred to below. MODIS/MISR performance in SA/MC can also be erratic (Reid et al., 2013–this issue).

Shown in Fig. 1 are mean annual (Fig. 1a) and seasonal CALIOP 0.532 μm AOD for 2007–2009 over SA/MC (defined here as 75° W/15° S–135° W/30° N). Seasonal means are derived for February–April (FMA; Fig. 1b), May–July (MJJ; Fig. 1c), August–October (ASO; Fig. 1d) and November–January (NDJ; Fig. 1e), chosen based on Reid et al. (2012) to best group dominant climate mechanisms/circulation with regional burning processes observed annually. CALIOP retrievals indicate higher AOD over land than over water, approaching a factor of five. The Bay of Bengal nearest the coastline is the lone exception. Seasonal variability is evident. During FMA, maximum values are observed over Myanmar, Thailand, Laos, Cambodia and southeastern China, reflecting a period of high burning activity locally favored by the position of the regional monsoonal trough (e.g., Reid et al., 2012a). Elevated values over China reflect urban activities and likely some dust components through advection from the sub-continent (i.e., Uno et al., 2009). During MJJ, high values are seen in the west, from India reaching out over the Bay of Bengal (e.g., Dey and Di Girolamo, 2011). Burning activity over the MC, including Sumatra, Java and Borneo Islands of Indonesia, corresponds with seasonal maximums found in those regions during ASO (e.g., Hyer and Chew, 2010; Reid et al., 2012a). The lowest seasonal values are observed during NDJ.

Evaluation of NAAPS skill and representativeness and an assessment of regional bias in SA/MC are described in Appendix A. The model exhibits reasonable stability for conducting comparisons with CALIOP, though caveats exist and are referred to within the narrative. Shown in Fig. 2 are

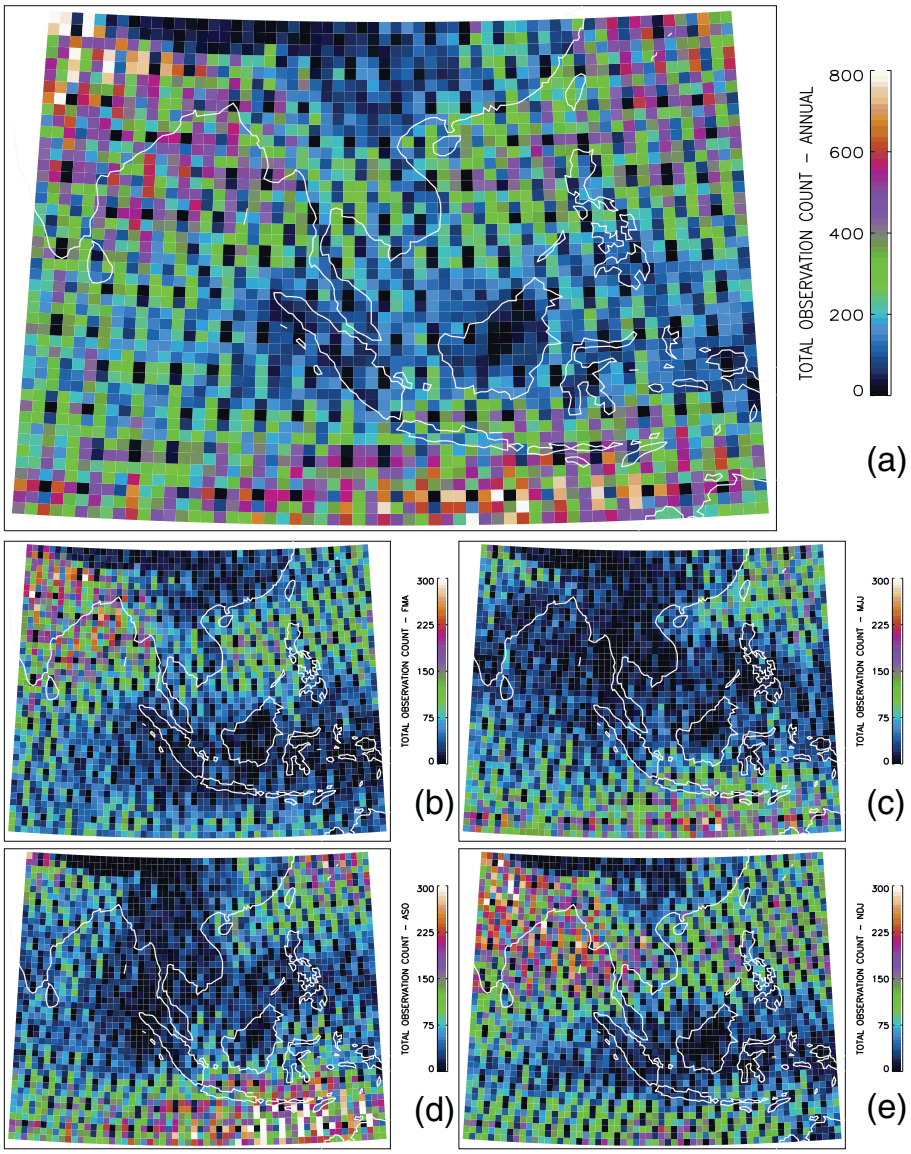

Fig. 3. Corresponding with Figs. 1 and 2, at 1°×1° resolution, sample counts for the (a) mean annual, (b) FAM, (c) MJJ, (d) ASO and (e) NDJ averages.

Table 1
For the 2007–2009 CALIOP and corresponding NAAPS sub-sample, mean AOD over land, coastal and ocean regions, and sample sizes, calculated both for all points inclusive and in a weighted format per 1°×1° NAAPS grid bin.

		Land		Coast		Ocean		Total	
		CALIOP	NAAPS	CALIOP	NAAPS	CALIOP	NAAPS	CALIOP	NAAPS
All data	Total	0.412	0.312	0.165	0.202	0.102	0.151	0.180	0.193
	Sample	142,679 (23%)		53,202 (9%)		417,592 (68%)		613,473	
Per bin	Total	0.310	0.235	0.129	0.153	0.086	0.124	0.155	0.159
	Sample	772 (29%)		286 (11%)		1642 (60%)		2700	

annual and seasonal mean ratios of CALIOP versus NAAPS AOD for all data points from 2007 to 2009. Sample counts per bin, both annually and seasonally, are shown in Fig. 3, corresponding with the composites in Figs. 1 and 2, as well as in Figs. 7–14 described below. Note that in Supplemental Fig. 1 (Fig. S1), those bins with zero sample counts are specifically depicted in order to lessen the ambiguity induced by the low end of the color bar in Fig. 3. Furthermore, in Table 1 are averages of CALIOP and corresponding NAAPS AOD over land, coastal regions and open ocean for 2007–2009, reported both for all data points inclusive and for a normalized sample where the average of each 1°×1° bin is treated as a single data point. This latter method compensates for varying distributions of available data points through the region.

Evident from Table 1 and Fig. 2a is that CALIOP AODs are high versus NAAPS over land, but relatively low over water. Areas of extremely high CALIOP values relative to the model are concentrated over southern India, northern Philippines, the southern Malay peninsula, central Sumatra and eastern Java, the latter corresponding with that of the urban Jakarta superplume. Mean CALIOP AODs over land/water are 0.412/0.102 for all data points inclusive, compared with 0.312/0.151 for NAAPS. When the average from each grid point is treated as a single data point, these values become 0.310/0.086 versus 0.235/0.124, respectively. Note, however, that total regional averages, 0.180/0.155 for all CALIOP data and the bin-normalized means, respectively, versus 0.193/0.159 for NAAPS, are remarkably consistent, though clearly a reflection of offsetting land/ocean biases regressing to a stable mean in the sum average. These results are encouraging. With exceptions in the far southwest corner of the region, no sector exhibits reasonably consistent CALIOP/NAAPS ratio values near unity. One area of exception, however, over land is the eastern Indo-Gangetic Plain, though NAAPS is unusually high there versus MODIS/MISR. A clear offset is found annually and seasonally at the regional coastlines. That is, CALIOP retrievals exhibit a strong AOD discontinuity between land and water in the SA/MC. This point is reexamined in Section 3.1.

CALIOP AOD retrievals are evaluated for seven SA/MC subsectors, which are outlined in Fig. 4 and defined in Table 2 as

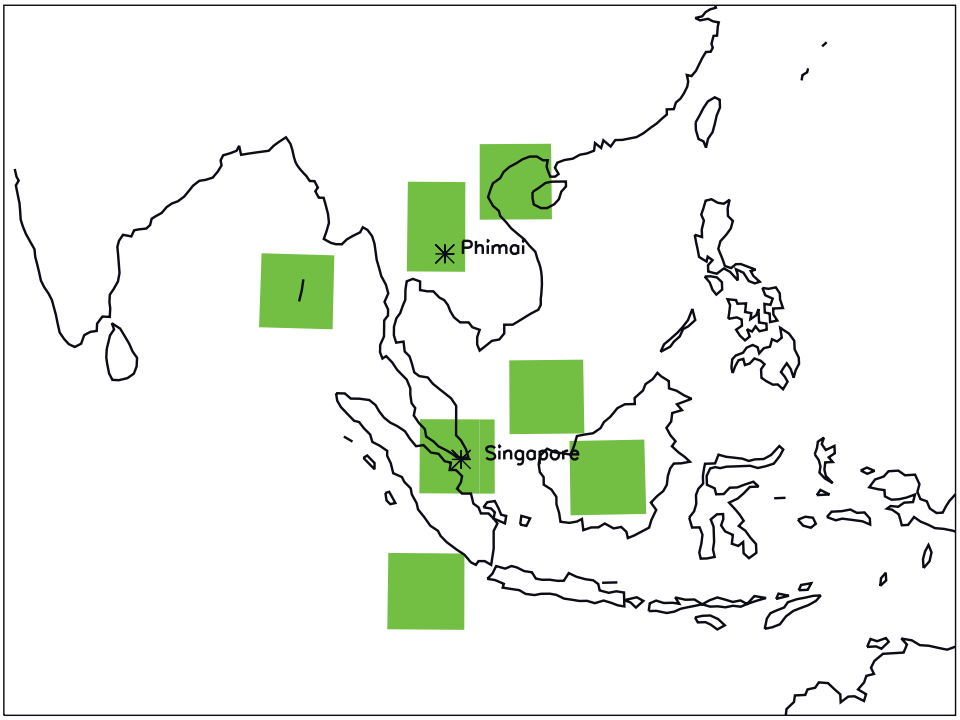

Fig. 4. SA/MC regional sub-sectors used for analysis in Table 2, and vertical profiling in Section 4, including Bay of Bengal, 90° E/10° N–95° E/15° N, Sumatra South, 99° E/10° S–104° E/5° S, Thailand, 100° E/14° N–104° E/20° N, Sumatra North, 101° E/1° S–106° E/4° N, Gulf of Tonkin, 105° E/17° N–110° E/23° N, South China Sea, 107° E/3° N–112° E/8° N, and Borneo, 111° E/3° S–116° E/3° N. Regional ground based lidar sites are also identified for Phimai, Thailand and Singapore (see Figs. 14 and 15 for coordinates).

Bay of Bengal, (90° E/10° N–95° E/15° N; BOB), Sumatra South (99° E/10° S–104° E/5° S; SS), Thailand (100° E/14° N–104° E/20° N; T), Sumatra North (101° E/1° S–106° E/4° N; SN), Gulf of Tonkin (105° E/17° N–110° E/23° N; GoT), South China Sea (107° E/3° N–112° E/8° N; SCS) and Borneo (111° E/3° S–116° E/3° N; B). Ground-based lidar sites, used for comparisons described in Section 4, are also identified. Table 2 includes mean CALIOP 0.532 μm AOD and retrieval uncertainties, corresponding NAAPS 0.550 μm AOD, RMSD and correlation coefficients solved between the two datasets, slope of each linear regression and its matching y-intercept coordinate, median, cloud-cleared QA sample size and total available L2-AProf 5-km data points before screening. Three of the domains are exclusively over water (BoB, SS and SCS), two over land (T and B) and two are mixed (SN and GoT).

Reiterating the finding described above, CALIOP AODs are higher in the over land sectors than NAAPS, lower over water, and lower for the two mixed regions. At BoB, CALIOP mean AOD is roughly one-third of NAAPS. At B, it is nearly 50% higher. Regression slopes reflect an alternating high/low bias. Interestingly, comparison of sample size versus total available data points, considered a proxy for regional cloudiness, indicates that over 60% of CALIOP L2-AProf observations are screened in all sub-sectors. At SN and B, this exceeds 80%, which is distinct in the regional sample count composites in Fig. 3, and reinforces how difficult the region is as a whole for profiling the aerosol system without concern for cloud contamination. Findings of simultaneous SA/MC high/low bias are generally consistent with a similar global analysis of CALIOP AOD retrievals versus co-located daytime-only MODIS retrievals (e.g., Remer et al., 2005, 2008) from the Aqua platform (i.e., part of the NASA EOS A-Train) for June 2006–August 2008 conducted by Kittaka et al. (2011). A similar study comparing CALIOP versus NAAPS by Campbell et al. (2012) also indicates such anomalies present in SA/MC.

3. CALIOP retrievals of aerosol particle composition, extinction coefficient and linear volume depolarization ratio

3.1. Aerosol particle composition: comparing CALIOP retrievals versus NAAPS speciation

Aerosol particle composition identified by the CALIOP algorithms is designated in the L2-AProf data file by the Atmospheric_Volume_Description variable for every 60 m profile bin. The six CALIOP aerosol particle types identified above are distinguished based on spectral scattering properties identified from both the visible and infrared instrument channels and linear depolarizing efficiencies at 0.532 μm (NASA, 2010; Omar et al., 2009). For 2007–2009, mean annual SA/MC CALIOP 0.532 μm AODs are shown in Fig. 5a–f for the six aerosol models, respectively (cases of 'other' are ignored here, as they contribute little to the overall signal). Each model represents a proxy for a range of physical and optical particle properties, including both fine and coarse mode partitioning, of size distribution, index of refraction, single scattering albedo and phase function (Omar et al., 2009), all of which are necessary inputs for initializing radiative transfer models.

Table 2
For 2007–2009 within each defined sector for at 1°×1° resolution grid averages, mean annual CALIOP 0.532 μm AOD, instrument/retrieval uncertainty (UNC.), corresponding mean annual NAAPS 0.550 μm AOD, root-mean square deviation (RMSD) between CALIOP and NAAPS, correlation coefficient between the two (CORL.), slope of the linear regression between the two (SLOPE), median of CALIOP AOD (Median) and sample size (Sample).

	Bay of Bengal 90 E/10 N–95 E/15 N	Sumatra South 99 E/10 S–104 E/5 S	Thailand 100/14 N–104 E/20 N	Sumatra North 101 E/1 S–106 E/4 N	Gulf of Tonkin 105 E/17 N–110 E/23 N	South China Sea 107 E/3 N–112 E/8 N	Borneo 111/3 S–116 E/3 N
CALIOP	0.1150	0.1059	0.3992	0.2586	0.3000	0.1017	0.3289
UNC.	0.0004	0.0004	0.0016	0.0020	0.0013	0.0006	0.0026
NAAPS	0.2302	0.1572	0.2917	0.2381	0.3218	0.1769	0.2761
RMSD	0.1859	0.1087	0.3205	0.2705	0.2868	0.1531	0.2915
CORL.	0.2762	0.4704	0.5614	0.3921	0.4838	0.3296	0.6273
Slope	0.3310	0.4397	0.7671	0.7729	0.8337	0.3137	0.6724
Coord.	0.0388	0.368	0.1754	0.0746	0.0318	0.0462	0.1432
Median	0.0769	0.0890	0.3006	0.1337	0.1669	0.0748	0.2144
Sample	6754	6578	4434	2386	4306	2918	1628
Total	19,699	18,686	15,149	13,402	16,194	14,373	10,315

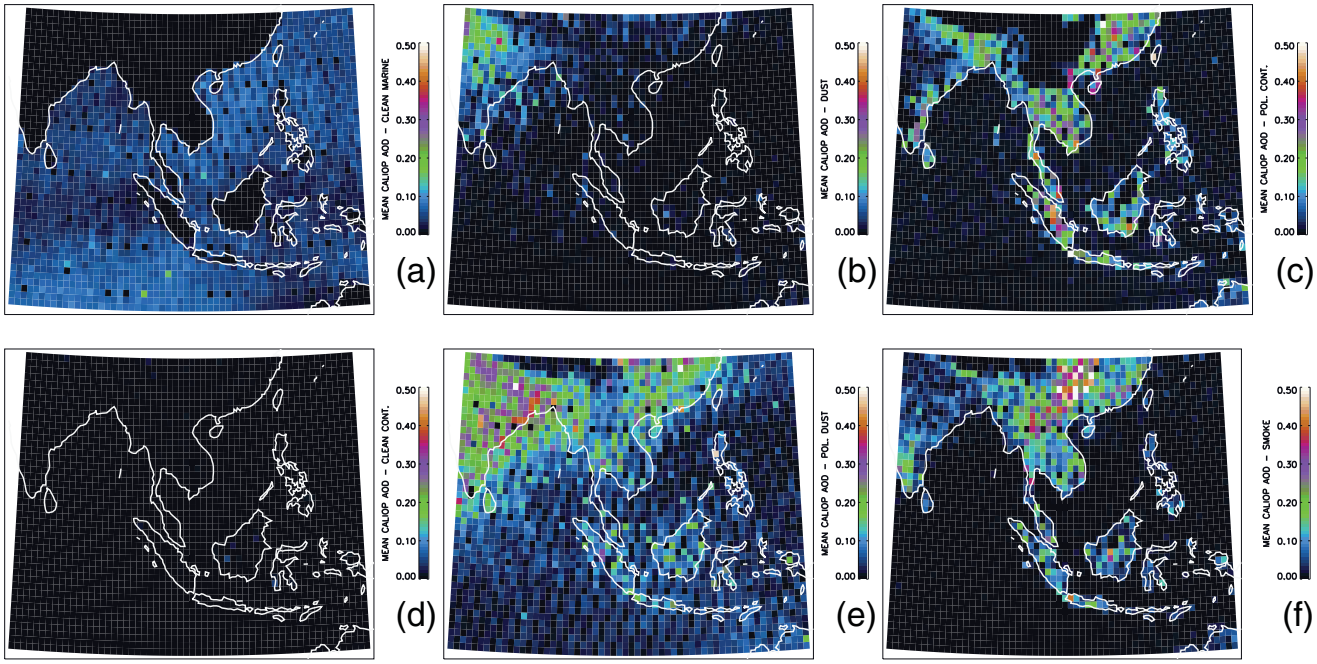

Fig. 5. For 2007–2009 at 1°×1° resolution, annual mean CALIOP-derived AOD for classified aerosol particle compositions, including (a) clean marine, (b) dust, (c), polluted continental, (d) clean continental, (e) polluted dust and (f) smoke.

Distinguishing composition through CALIOP represents a nascent but potentially ground-breaking attempt at an operational active-based satellite particle typing scheme. Some passive satellite remote sensors are used for differentiating fine and coarse mode particle fractions and varying composition, and exhibit reasonable skill (e.g., Omar et al., 2009). Practical limitations apply, however, particularly in cloudy regions like SA/MC (e.g., Kaufman et al., 1997b; Mischenko et al., 2007). Multi-sensor techniques improve the scenario (El-Askary et al., 2006), but can be difficult to synergize operationally over broad spatial and temporal scales. Active-remote sensors benefit from range-resolved scattering that is decoupled from any surface background reflectance, which simplifies basic macrophysical distinctions while retaining information as a function of height. Since CALIOP is an elastic-backscatter lidar, however, the indirect retrieval of the extinction coefficient is a potential limiting factor (e.g., Omar et al., 2009), thus creating a mechanism for high/low bias identified in Section 2 that can be investigated here for impact and, perhaps, motivated for future improvements.

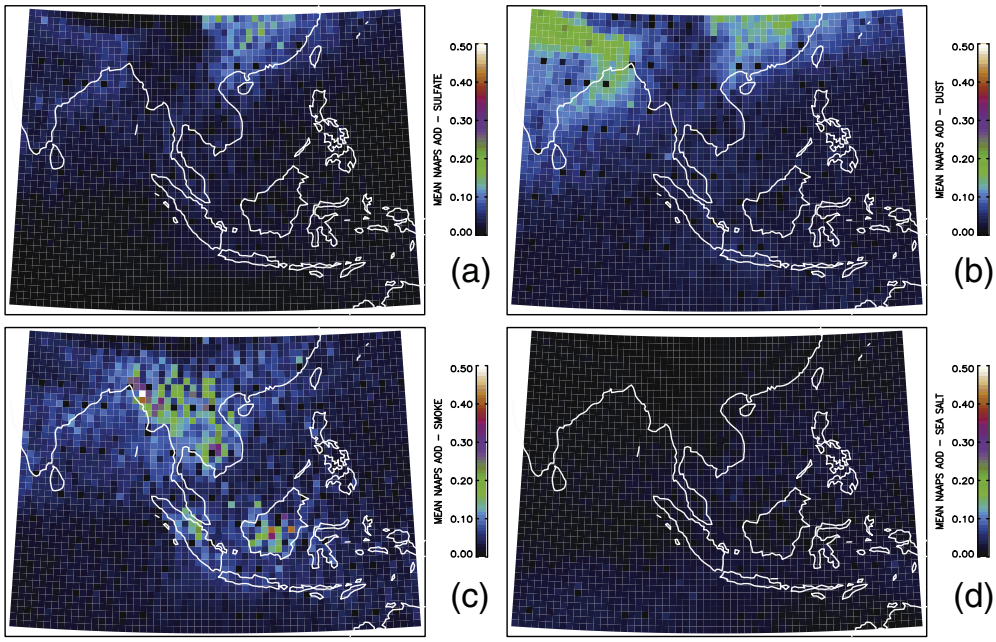

Fig. 6. For 2007–2009 at 1°×1° resolution, annual mean NAAPS-derived AOD for corresponding CALIOP data points and specific model aerosol particle compositions, including (a) sulfate, (b) dust, (c) smoke and (d) sea salt.

It is evident that CALIOP algorithms only identify some SA/MC species in significant amounts over land or water exclusively (Fig. 5), which likely contributes to the delineation of AOD found along the regional coastlines. Clean marine particles contribute to AOD only over water, which is reasonable. Clean continental aerosol particles contribute only a small fraction to regional AOD overall. Given the ubiquity of high AOD loadings in the region (Reid et al., 2013–this issue), these can be ignored for this discussion. The two dust categories are represented over both land and water. However, no significant AOD contribution is found over water for polluted continental and smoke types, though smoke, for instance, is readily found in over–ocean CALIOP data in other global regions (e.g., Yorks et al., 2009). Omar et al. (2009) report that only in the Arctic are specific aerosol types allowed or disallowed. They also state that all elevated non-depolarizing (LVDR<0.20) aerosols over-ocean are considered smoke. As will be shown in Section 3.2, smoke is predominant in SA/MC at low levels, though this very likely isn't being accurately reflected in CALIOP retrievals. Therefore, it is not clear that the smoke model is being applied representatively, and that this may be the cause of its underestimated presence over water in SA/MC, and perhaps contribute significantly to the underestimation of AODs found there, as well.

For comparison, mean NAAPS 0.550 μm AODs are shown in Fig. 6a–d, respectively, for relative contributions from sulfate, dust, smoke, and sea salt particles. Model speciation in this instance does not represent absolute truth, but instead a general guideline for evaluating the CALIOP retrievals. Over land, including India and the northern portion of the SA domain, NAAPS resolves more dust than the CALIOP retrievals. Of course, NAAPS components must be converted in weighted proportions for simulating the CALIOP mixtures (i.e., polluted dust and polluted continental). This finding is still significant, however, and relatively consistent. Based on a-priori assignment of the lidar ratio, dusts exhibit lower values than more absorptive mixtures and/or relatively smaller inherent particle distributions, as observed with carbon and sulfate residues (Ackerman, 1998; Liu et al., 2008). Thus if CALIOP retrievals are

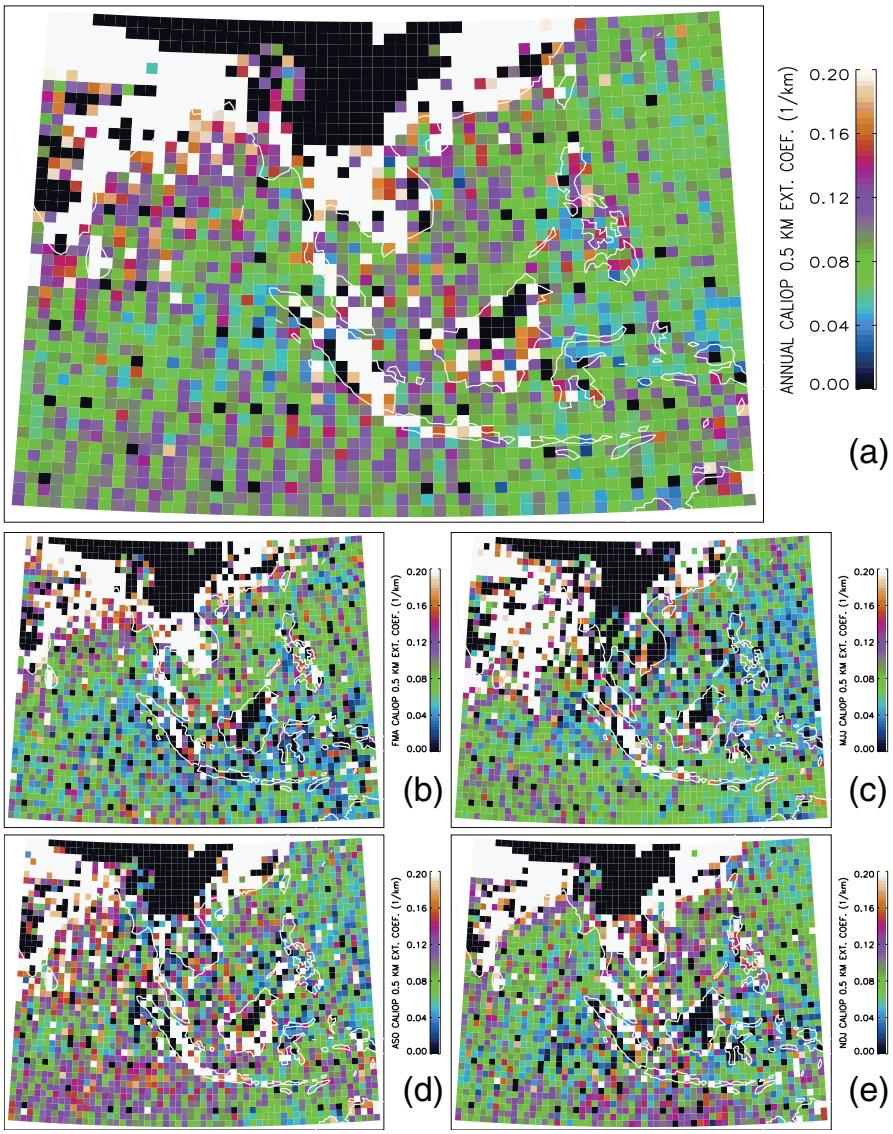

Fig. 7. For 2007–2009 at 1°×1° resolution, mean CALIOP-derived extinction coefficient (km^{-1}) solved at 0.50 km above mean sea level (a) annually, and for (b) FAM, (c) MJJ, (d) ASO and (e) NDJ, respectively.

conducted more predominantly with the mixtures, like polluted dust (65 sr versus 40 sr for dust at 0.532 μm in Version 2.01 data; Omar et al., 2009; now 55 sr for Version 3.01 data; M. A. Vaughan personal communication, 2011), the prescribed value will be biased high, aliasing retrieved AOD, accordingly. Similarly, over ocean, NAAPS indicates more regional smoke than identified from CALIOP. Considering the additional lack of polluted continental occurrence over ocean (both are assigned lidar ratios of 70 sr for CALIOP at 0.532 μm; the highest of the six defined species), the opposite scenario is likely occurring. Absorptive particles are not being accurately represented in lidar ratio selections, the value is thus biased low and retrieved AOD is low.

3.2. CALIOP 0.532 μm extinction coefficient on five vertical levels

Mean 2007–2009 CALIOP 0.532 μm extinction coefficient values are shown annually and seasonally for SA/MC on five levels (0.50, 1.50, 2.50, 3.50 and 4.50 km MSL) in Figs. 7–10 and Supplemental Fig. 2 (Fig. S2), respectively. Apparent data gaps, either single or multi-bin, in these composites are the result of two factors. First, the CALIPSO ground-track causes the instrument to miss profiling some 1°×1° grid sectors, leaving no data available for analysis (the interested reader is again referred to Fig. S1 for a depiction of these bins). This was equally apparent in Figs. 1, 2, 4 and 5. However, a second factor arises here from topography, which is complicated in northern SA approaching the Himalayas and Tibetan Plateau and to the south over Borneo. No data are reported when the height of the surface exceeds the level of interest.

At 0.50 km MSL annually, most low-land areas are subject to extinction coefficient values at or exceeding 0.20 km^{-1}. Much of the terrain, however, particularly to the north, is situated above this level. Some lower values are apparent near the coastlines. Over open waters, the scene is more persistent, though outflow into the northern Bay of Bengal, northern Indian Ocean southwest of Sumatra, and western South China Sea are apparent. At this level, topography, thermal inversions

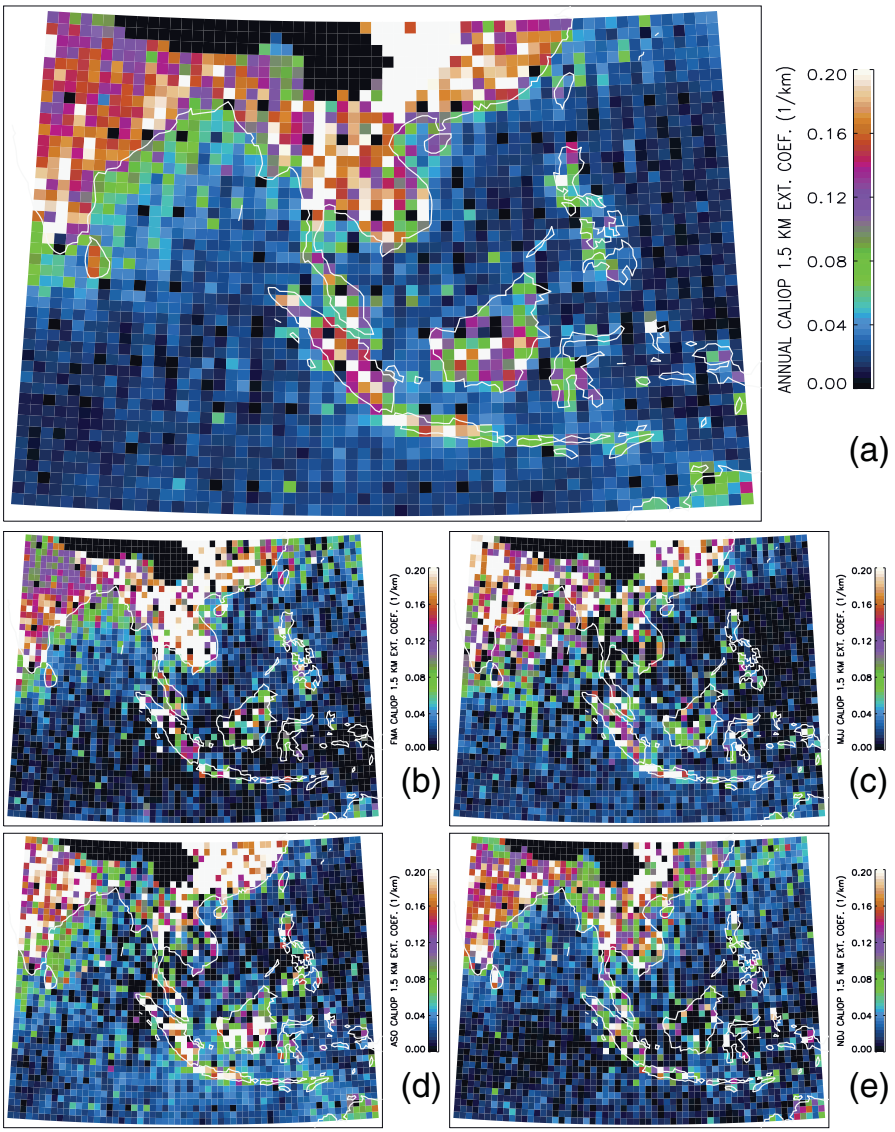

Fig. 8. For 2007–2009 at 1°×1° resolution, mean CALIOP-derived extinction coefficient (km^{-1}) solved at 1.50 km above mean sea level (a) annually, and for (b) FAM, (c) MJJ, (d) ASO and (e) NDJ, respectively.

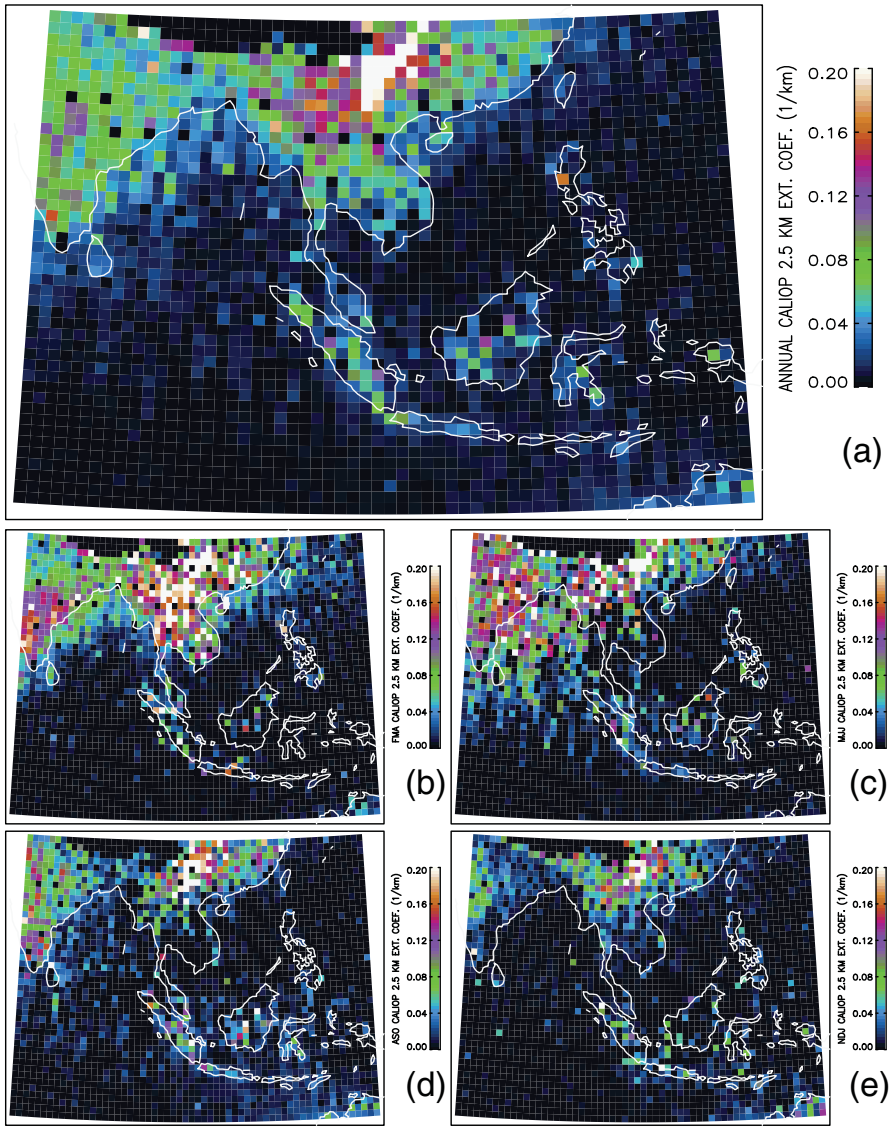

Fig. 9. For 2007–2009 at 1°×1° resolution, mean CALIOP-derived extinction coefficient (km^{-1}) solved at 2.50 km above mean sea level (a) annually, and for (b) FAM, (c) MJJ, (d) ASO and (e) NDJ, respectively.

and the disparity of local anthropogenic sources influence the presence and concentration of aerosol particles, in contrast with elevated levels where transport dominates and spatial autocorrelation lengths increase (Anderson et al., 2003b; Zhang et al., 2008).

Seasonally, Indian continental outflow into the Bay of Bengal is strongest during MJJ (Fig. 7c) and ASO (Fig. 7d). Regional burning on the Indochinese Peninsula (i.e., Myanmar, Thailand, Malaysia, Cambodia, Laos and Vietnam) is maximum during January–April (Giglio et al., 2006; Reid et al., 2012a; Hyer et al., 2013–this issue), and found as elevated values there in the NDJ (Fig. 7e) and FMA (Fig. 7b) composites. Elevated values in the southeastern quadrant (i.e., northeastern Indian Ocean), particularly during ASO, represents advection along trajectories from burning and urban industrial anthropogenic sources on Sumatra and Java (Xian et al., 2013–this issue). These same sources, and now including burning in southern Malaysia and Borneo, combine with an increasing favorability for anticyclonic circulation during ASO and NDJ to increase values over the South China Sea (Xian et al., 2013–this issue).

Annually at 1.50 km MSL, delineation between over-land and over-ocean values remains distinct (Fig. 8a). Over land, values approach and exceed 0.20 km^{-1} in many areas. Seasonal distributions vary less noticeably. Outflow into the Bay of Bengal is strongest again during MJJ (Fig. 8c). Conspicuously, whereas outflow from Sumatra and Java can be seen during ASO into the northeastern Indian Ocean (albeit at values below 0.05 km^{-1}, though still above background values), values over the South China Sea are low. Observations from local ground-based lidar, described in Section 4, depict a slightly larger elevated component than CALIOP. Whether or not CALIOP representativeness is in question, or if this result comes from biased a-priori lidar ratio determination, the result is potentially significant. Despite a convective tropical environment and active regional burning, and thus the apparent buoyancy and mixing necessary to loft matter into the free troposphere, CALIOP measurements indicate that the bulk of the aerosol

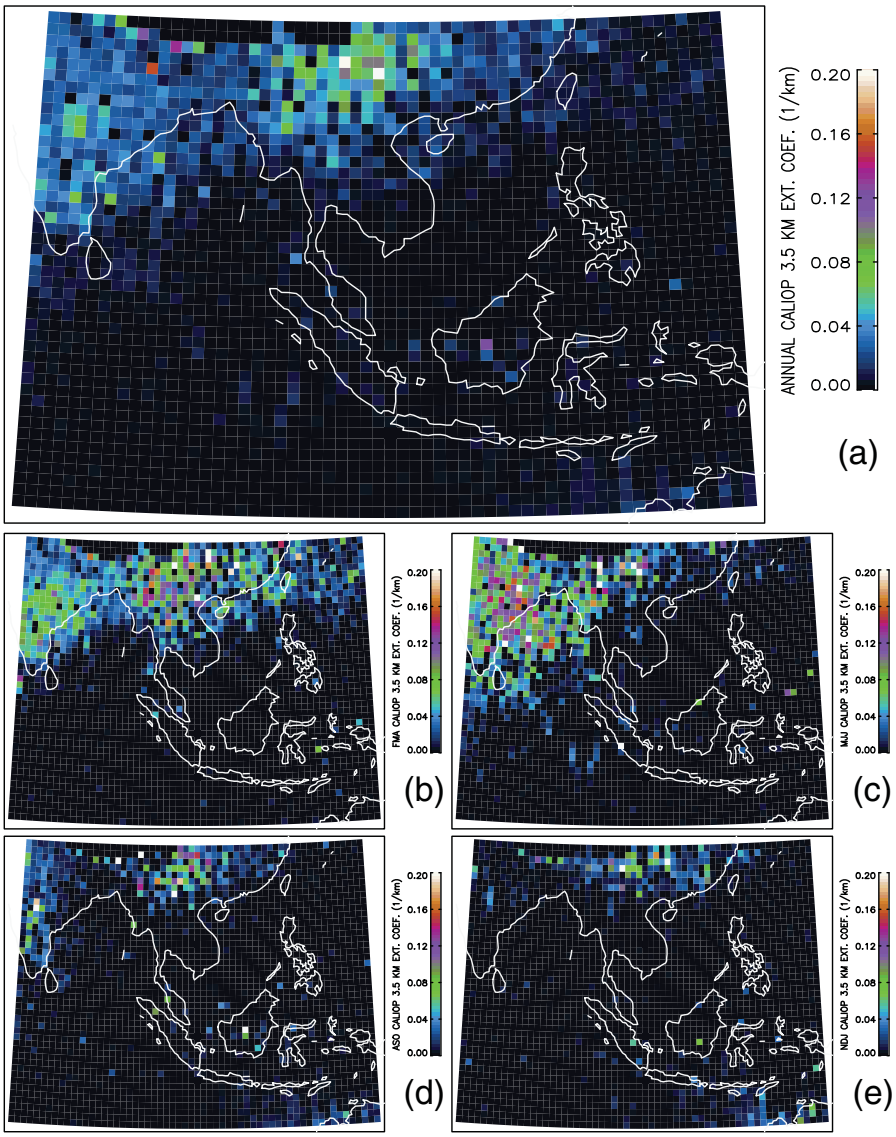

Fig. 10. For 2007–2009 at 1°×1° resolution, mean CALIOP-derived extinction coefficient (km^{-1}) solved at 3.50 km above mean sea level (a) annually, and for (b) FAM, (c) MJJ, (d) ASO and (e) NDJ, respectively.

particle scattering over the waters of the MC is effectively capped below 1.5 km MSL, and thus elevated outflow from land sources is being suppressed.

By 2.50 km MSL, increasing persistence is apparent annually (Fig. 9a). An exception to this occurs southeast of the Tibetan Plateau over southeastern China, northern Laos and northern Vietnam. This is believed attributable to advection off of the plateau, and of regional springtime burning from northern Thailand and Myanmar. Values in this area are highest, approaching and exceeding 0.15 km^{-1} on average. Compared with lower levels, values are very low over the MC. Only over the islands of Sumatra, Java, Borneo, and Sulawesi, do they approach 0.08 km^{-1}. Seasonally, the burning season over the Indochinese Peninsula causes maximum values found there during FMA (Fig. 9b). Otherwise, that sector, particularly to the south, exhibits relatively low values during the remainder of the year. The highest values are instead oriented along the southeastern corner of the plateau. Outflow from India over the Bay of Bengal during FMA (Fig. 9b) is again apparent at this height. Fire season in the southern MC, over Sumatra and Borneo is identified during ASO (Fig. 9d). However, elevated outflow over open MC waters is again constrained. Very low values are found over the South China Sea and northeastern Indian Ocean.

At 3.50 km MSL, significant aerosol particle presence is confined to the northwestern and central sections of the region, with maximum annual mean values capped near 0.08 km^{-1} (Fig. 10a). The highest values are found along the southeastern edge of the Tibetan Plateau, while more diffuse structure reaches westward over India. Surface mechanisms responsible for this distribution are likely similar to those found at 2.50 km MSL. Fire season over the northern Indochinese Peninsula during FMA results in elevated values there relative to the annual mean (Fig. 10b). Indian outflow over the Bay of Bengal is present during MJJ (Fig. 10c). However, the MC region exhibits effectively no significant aerosol presence at this level, even during that region's primary burning season in ASO (Fig. 10d). By 4.50 km MSL (Figs. S2a–e), the only significant signals found

are over India with limited associated outflow over the northern Bay of Bengal during MJJ.

3.3. CALIOP 0.532 μm linear volume depolarization ratio on five vertical levels

When irradiated by a polarized source, the shape of the scatterer influences the resulting polarization state of the 180° backscattered component. Solution-based aerosol particles exhibit negligible depolarization relative to the incident polarization state since the coaxial reflection off of the rear droplet face dominates total backscatter (Sassen, 1991). In contrast, many solid aerosol particle types, most notably dust, regularly depolarize as 180° scattering is dominated by internal particle reflections (Sassen, 1991). LVDR, defined as the ratio between energy measured in the perpendicular polarization state and that in the state parallel relative to the outgoing pulse (Schotland et al., 1971), including the volume-normalized contribution of molecular scattering, has become a reliable measurement for the qualitative interpretation of aerosol microphysical properties (e.g., Liu et al., 2004; Sassen, 2005), and has been more recently related to scattering processes in the atmosphere (Mishchenko and Hovenier, 1995; Flynn et al., 2007; Gimmestad, 2008).

Mean annual and seasonal 2007–2009 CALIOP 0.532 μm LVDR values are shown for SA/MC on the same five levels applied for extinction coefficient. The 0.50 km MSL level is shown in Fig. 11, continuing for the 1.50 km MSL level in Fig. 12, 2.50 km MSL in Fig. 13, and 3.50 km MSL in Fig. 14. Values at 4.50 km MSL are again provided for the interested reader in Supplemental Fig. 3 (Fig. S3). As described in Section 2, only those LVDR values are analyzed when a bin corresponds with aerosol particle presence. Otherwise, values indicative of clear air would bias the sample, limiting the interpretation. Thus in contrast with extinction coefficient composites (Figs. 7–10) above, these data exhibit more noise with increasing height.

The 0.50 and 1.50 km MSL composites depict relatively consistent LVDR distributions and seasonal variability. Annually (Figs. 11a and 12a, respectively), regional mean values are

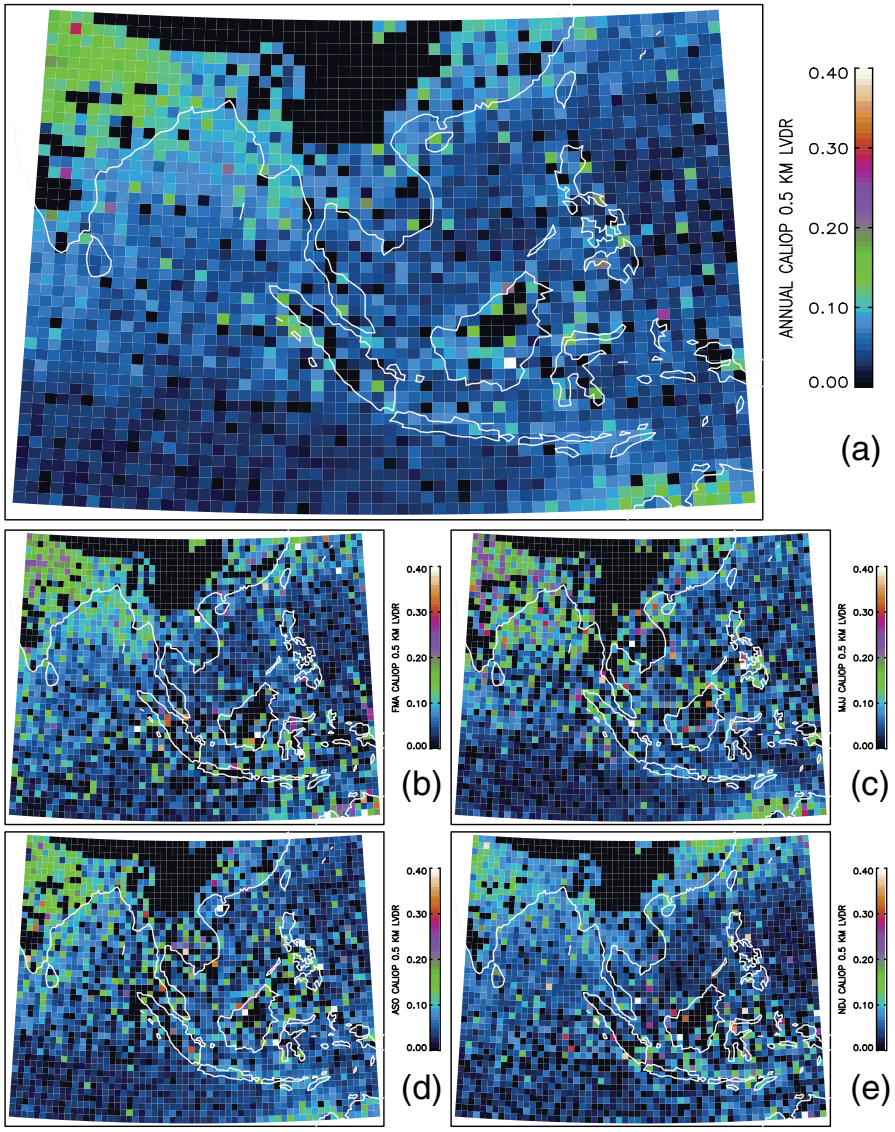

Fig. 11. For 2007–2009 at 1°×1° resolution, mean CALIOP-derived linear volume depolarization ratio (LVDR; unitless) solved at 0.50 km above mean sea level (a) annually, and for (b) FAM, (c) MJJ, (d) ASO and (e) NDJ, respectively.

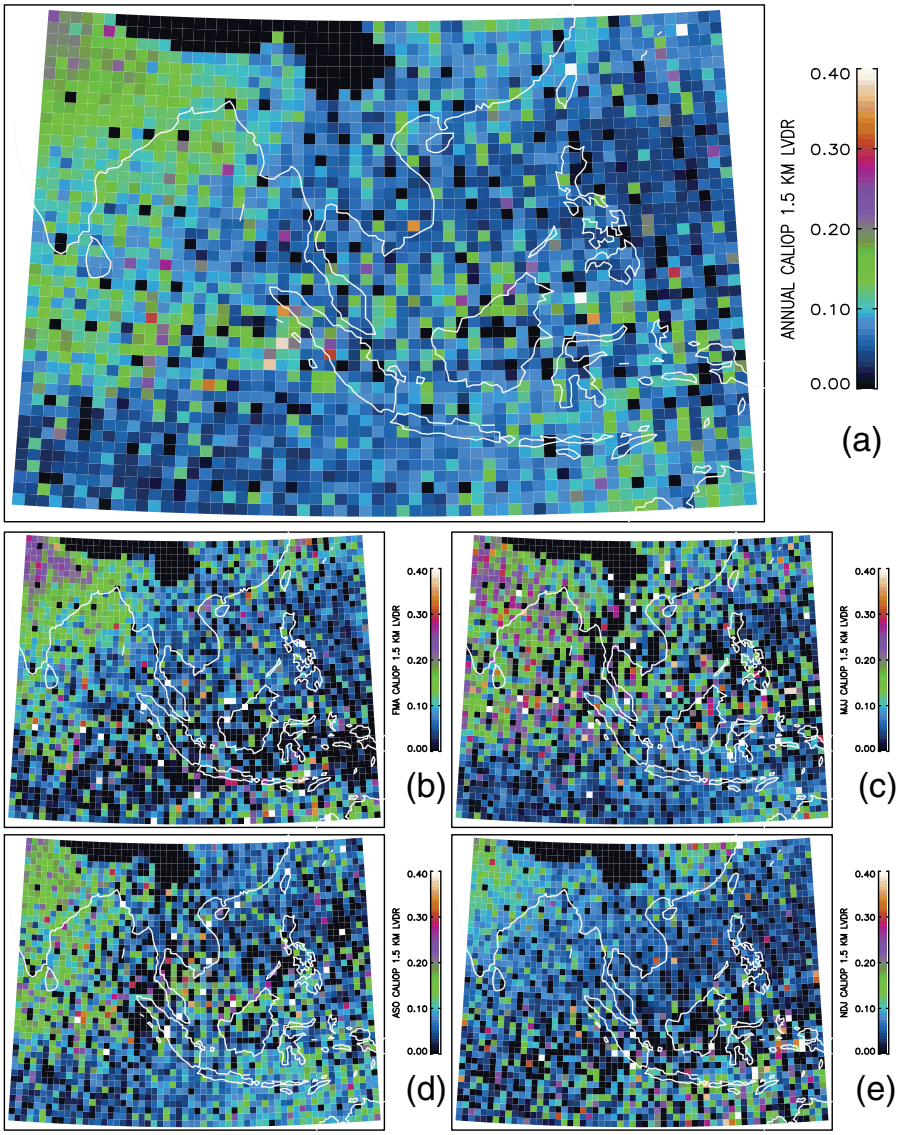

Fig. 12. For 2007–2009 at 1° × 1° resolution, mean CALIOP-derived LVDR (unitless) solved at 1.50 km above mean sea level (a) annually, and for (b) FAM, (c) MJJ, (d) ASO and (e) NDJ, respectively.

near 0.10. Higher values, approaching 0.15, are found over India to the west, and increasingly in continental outflow over the Bay of Bengal at 1.50 km MSL. Over western SA and nearly the entire MC, values are 0.10 on average or lower. These data indicate that near the surface more spherical particles are present, reflecting enhanced particle deliquescence (Adachi et al., 2011), which is consistent for a tropical maritime environment, and the likely predominance of anthropogenic haze, fresh smoke and sea salt aerosol particles. This also reinforces interpretations made earlier comparing CALIOP speciation with NAAPS (Figs. 5 and 6) that the depiction of dust and polluted dust concentrations (i.e., depolarizing particles) over the MC and surrounding waters is likely anomalous, and biasing low satellite AODs. More smoke is likely present in these areas than what the algorithms are identifying. This is important given that most aerosol particle extinction is found at and below 1.5 km MSL (Figs. 7 and 8). The effect of sea salts, which typically exhibit very low relative lidar ratios (Ackerman, 1998), however, is unknown. As they also induce very little depolarization, it will be relevant in future studies aimed at reconciling MC smoke concentrations to determine what effect sea salts play on the marine aerosol system regionally and with increasing height.

Seasonal LVDR at 0.5 and 1.5 km MSL are mostly consistent with distributions of regional sources identified when interpreting extinction coefficient values above. The signal for regional burning over the Indochinese Peninsula during FMA (Figs. 11b and 12b) corresponds with relatively low LVDR. This is reaffirmed during ASD (Figs. 11d and 12d) for the islands of the MC, where again relatively low values are seen, as well as along outflow trajectories over the northern Indian Ocean and South China Sea. An axis delineating elevated LVDR in the north from lower values in the south reaches from Sri Lanka northeastward toward Taiwan during MJJ (Figs. 11c and 12c) and NDJ (Figs. 11e and 12e). This feature is more pronounced at 1.5 km MSL. As these two periods represent relatively quiet periods for regional burning in the north (FMA maximum) and south (ASO maximum; Giglio et al., 2006; Reid et al., 2012a;

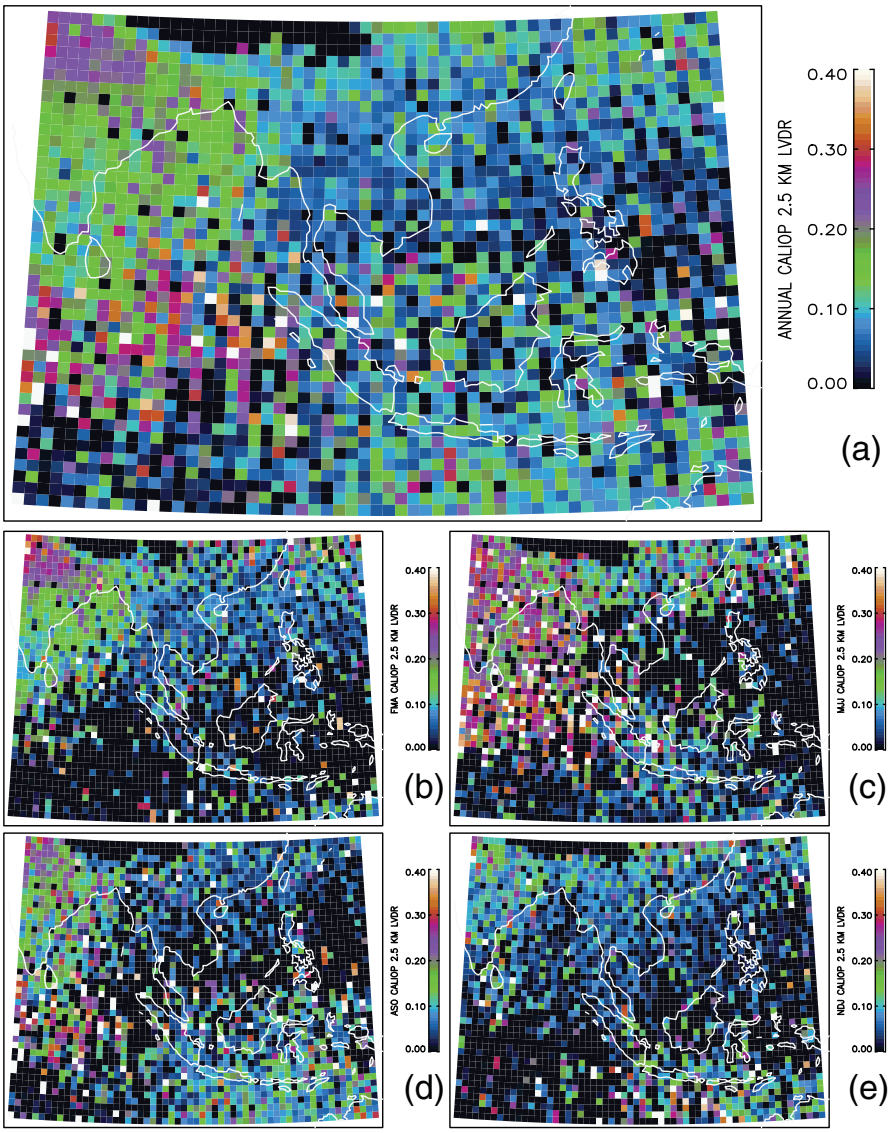

Fig. 13. For 2007–2009 at 1°×1° resolution, mean CALIOP-derived LVDR (unitless) solved at 2.50 km above mean sea level (a) annually, and for (b) FAM, (c) MJJ, (d) ASO and (e) NDJ, respectively.

Hyer et al., 2013–this issue), it's likely that lesser amounts of smoke present result in higher mean LVDR from a predominance of dusts and other aspherical anthropogenic particles during these periods.

At elevated levels, the scene is more complicated. Annually at 2.5 km MSL (Fig. 13a), higher values (>0.10) are found in the west over India and through outflow over the Bay of Bengal and far northern Indian Ocean. In the east, values are generally near 0.10 near land, except over southeastern China where they increase. At 3.5 km MSL (Fig. 14a), little data is available from southwest to northeast across the MC and South China Sea. Very high values are instead found over India and the Bay of Bengal, the highest of which occurs during MJJ (Fig. 14c). By 4.5 km MSL (Fig. S3), the only significant signals are found in bands of higher values over the northern land sector, with the highest of those occurring during MJJ (Fig. S3c) and no significant signal found during ASO (Fig. S3d) or NDJ (Fig. S3e). These data reflect the increasing predominance of dust occurrence with height. Over land, however, recall that NAAPS resolves more dust than CALIOP, particularly over southeastern China. CALIOP algorithms are classifying aerosol particles there more frequently as polluted dust. LVDR near the surface, however, is relatively low (<0.10). The corresponding presence of elevated dust in these regions thus indicates a potential decoupling of elevated particle layers relative to sources and advection stratified within the near-surface layer that may complicate classification by CALIOP algorithms.

Over the far-southern MC, an area of correlated signals is distinct at 2.5 km MSL with LVDR on average near 0.10. An equivalent response in mean extinction coefficient (Fig. 9a) is more difficult to distinguish from the signal originating over Sumatra, Java and Borneo. This becomes more distinct at 3.5 km MSL (Fig. 14a). By 4.5 km MSL (Fig. S6a), it no longer appears. Seasonally, elevated values at 3.5 km MSL correspond with the ASO (Figs. 13d and 14d) and NDJ (Figs. 13e and 14e) seasons. It is not clear what the source of these particles/signals is. There is the potential for transport from Australia. Active volcanoes on the Indonesian islands could also be responsible,

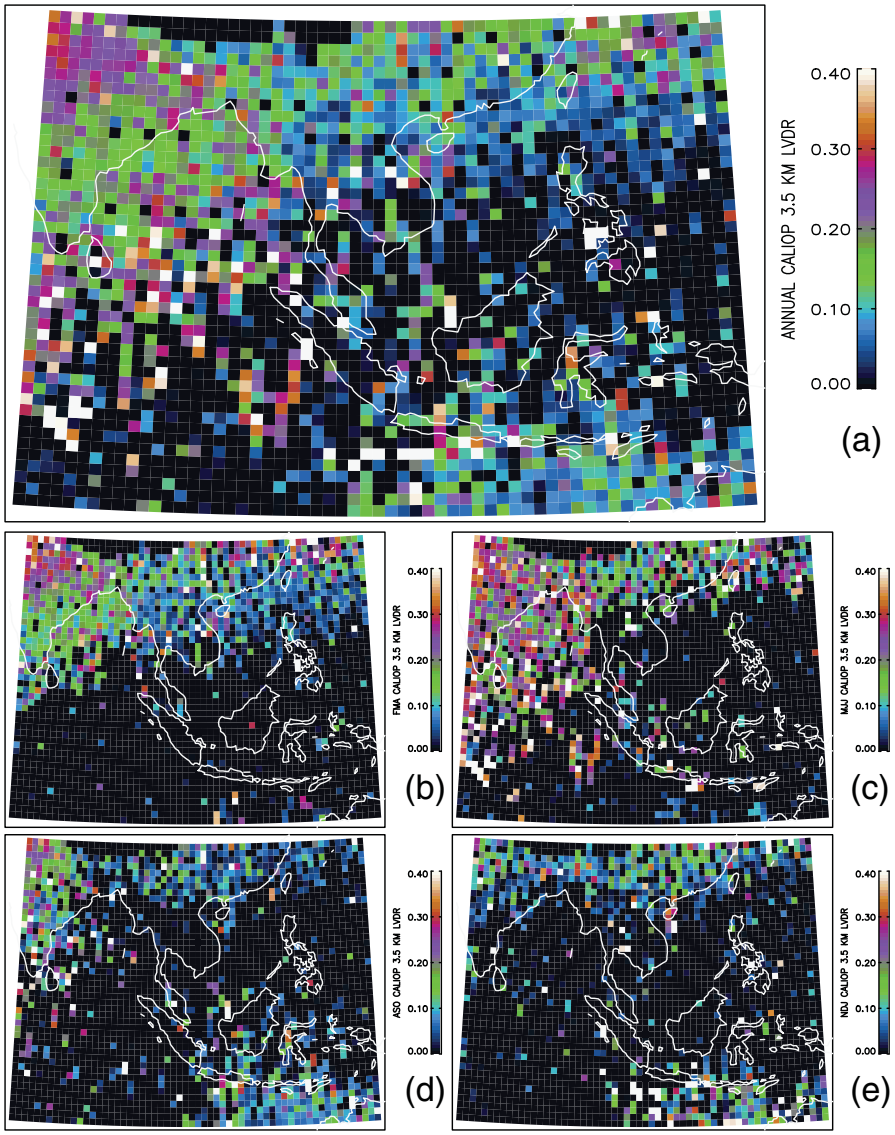

Fig. 14. For 2007–2009 at 1° × 1° resolution, mean CALIOP-derived LVDR (unitless) solved at 3.50 km above mean sea level (a) annually, and for (b) FAM, (c) MJJ, (d) ASO and (e) NDJ, respectively.

given the propensity for ash to depolarize (Sassen et al., 2007), though no major eruptions occurred during the 2007–2009 period. Furthermore during ASO, LVDR are near and below 0.10. During NDJ, they are generally higher, exceeding 0.15, on average, which complicates the identification of a likely source further.

4. Vertical profiles of CALIOP 0.532 μm extinction coefficient compared with ground-based lidar measurements

Returning to the seven designated SA/MC sub-sectors, ground-based lidar measurements of aerosol particle extinction coefficient are considered from February 2008 to January 2009 at Phimai, Thailand (0.532 μm; 15.2° N, 102.6° E, 212 m MSL) and November 2009–December 2010 at Singapore (0.527 μm; 1.30° N, 103.77° E, 79 m MSL; Fig. 4). Mean annual and seasonal CALIOP 0.532 μm extinction coefficient profiles are thus shown for the T and SN sub-sectors, respectively in Figs. 15 and 16, versus the corresponding ground-based profiles. These ground-based measurements are similarly cloud-cleared, and also reflect indirect retrievals, since like CALIOP they measure elastic backscatter. Observation periods do not match the CALIOP subset directly. However, they represent the bulk of the data archive available from each site, and will be interpreted with this caveat in mind. CALIOP-derived extinction coefficient profiles for the other five SA/MC sectors are presented and described by Reid et al. (2013–this issue).

The Phimai instrument is deployed by the Japanese National Institute for Environmental Studies (NIES) as part of Skynet (http://atmos.cr.chiba-u.ac.jp/), which includes a co-located multi-channel sky radiometer on site (Shimizu et al., 2004; Aoki, 2008; Nishizawa and Sugimoto, 2009). Data are recorded and reported here at 30 m vertical resolution. The Singapore site is coordinated by the NASA Micropulse Lidar Network (http://mplnet.gsfc.nasa.gov/; Welton et al., 2001; Campbell et al., 2002), with an AERONET sun photometer operated less than 1 km away. Data from this instrument are Level 2 quality-assured and reported at 75 m vertical resolution. At Phimai, aerosol particle

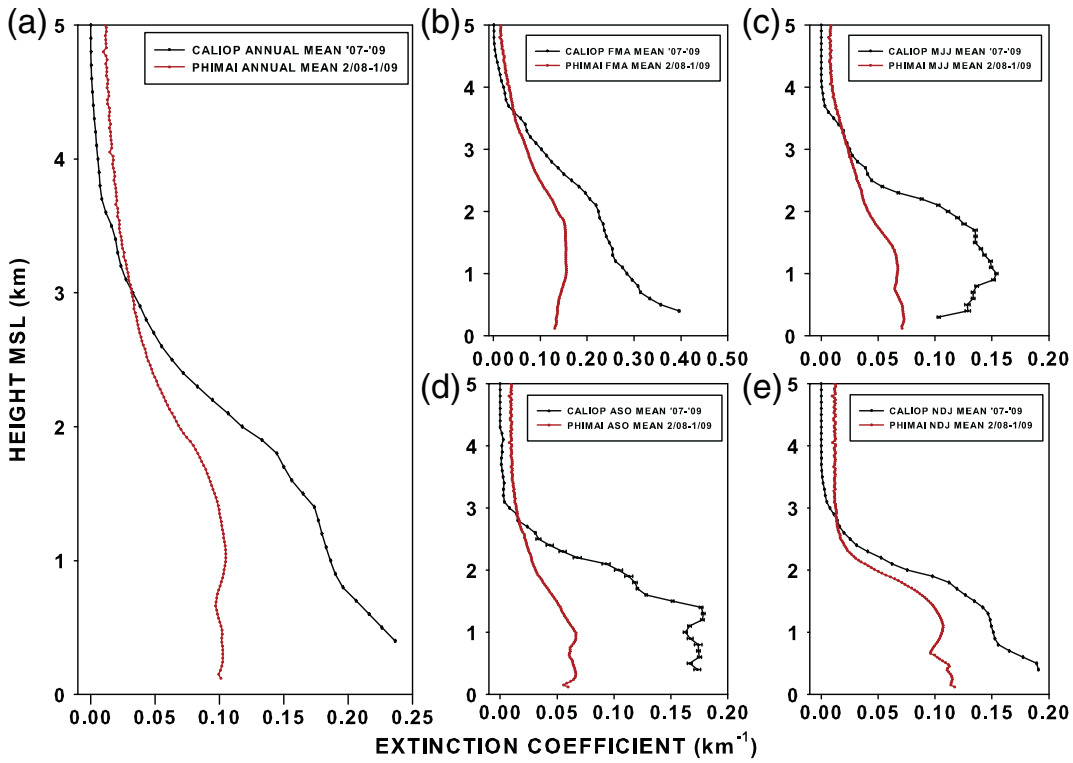

Fig. 15. For the Thailand sector (Fig. 4; Table 2; 100° E/14° N–104° E/20° N) (a) 2007–2009 mean annual 0.532 μm CALIOP extinction coefficient profile and mean February 2008–January 2009 Skynet 0.532 μm extinction coefficient profile collected at Phimai, Thailand (see inset; 15.2° N, 102.6° E, 212 m MSL), with corresponding seasonal averages for (b) FMA, (c) MJJ, (d) ASO and (e) NDJ.

extinction coefficient is solved by parameterizing the lidar ratio at a constant 50 sr. For MPLNET, it is solved by constraining an iterated solution using co-located AOD measurements (e.g., Fernald, 1984; Welton et al., 2002). Uncertainties are not shown for either ground-based dataset, as the subsequent analysis is predominantly qualitative.

Comparisons of Phimai measurements with the CALIOP subset are relatively coarse. The dimensions of the T sector chosen, however, stretch from the central–southern urban areas northward over forests and highlands, where burning is more comprehensive and AOD is higher (Reid et al., 2013–this issue; Fig. 15a). Differences are to be expected. CALIOP AOD is only ~15% higher than NAAPS in this region (Table 2). However, this comparison leaves the impression of a much higher overestimate, nearing a factor of two annually and nearly four during ASO (Fig. 15d). Both instruments depict the effective top height of the aerosol layer near 2.5 km MSL, except for CALIOP during MJJ (Fig. 15c), where a significant elevated particle component is apparent. The bulk of the aerosol particle extinction is found below 2.0 km MSL by both instruments.

In Supplemental Fig. 4, comparisons of AOD retrievals from the Phimai lidar, and its prescribed lidar ratio, versus the Skynet sky radiometer are shown. The lidar retrievals here are consistently low by 5–30% seasonally during 2008–2009, suggesting that 50 sr, though reasonable, is effectively low. Furthermore in Fig. 17a–b, the fractional contribution to total and seasonal CALIOP extinction is shown for each of the six discrete aerosol types, as well as cases for 'other', used for assigning the a-priori lidar ratio used in the T and SN retrievals, respectively. As described above, the potentially anomalous use of the "polluted dust" model over land, compared with pure dust, may be contributing to a high bias in these data. Smoke is contributing very little below 2.0 km, which runs contrary to surface observations and regional processes, but is consistent with methods described above for its priority use for elevated layers.

At Singapore, the annual MPLNET profile is more consistent with CALIOP (Fig. 16a). From Table 1, CALIOP and NAAPS AOD are reasonably consistent in the SN sub-sector (0.26 versus 0.24, respectively), which is drawn roughly half over land and half over water (Fig. 4) and thus the mean profile is believed reflective of offsetting over-land/water algorithm tendencies described above. Both instruments indicate the bulk of significant aerosol particle extinction occurring below 3.0 km MSL. However, MPLNET resolves slightly more elevated structure near and above 1.5 km MSL during FMA and NDJ than does CALIOP. Again, however, these are different years being compared, so some differences are expected. MPLNET profiles also depict a well-defined surface layer top during all seasons, though most clearly evident during NDJ (Fig. 16e), that represents a likely decoupling of the marine environment from the airmass above.

Stratification of particle composition in this sector would again complicate a-priori assignment of lidar ratio and subsequent CALIOP retrievals of aerosol particle extinction coefficient. Considering the fractional contribution of the CALIOP aerosol models to total extinction shown in Fig. 17b, and similar to that seen at T, the magnitude of the "polluted dust" contribution again seems unusual. Particle asphericity at lower levels is not necessarily complex, seen from LVDR plots discussed above and considering a lack of corresponding regional sources. Furthermore, again, smoke is not well-

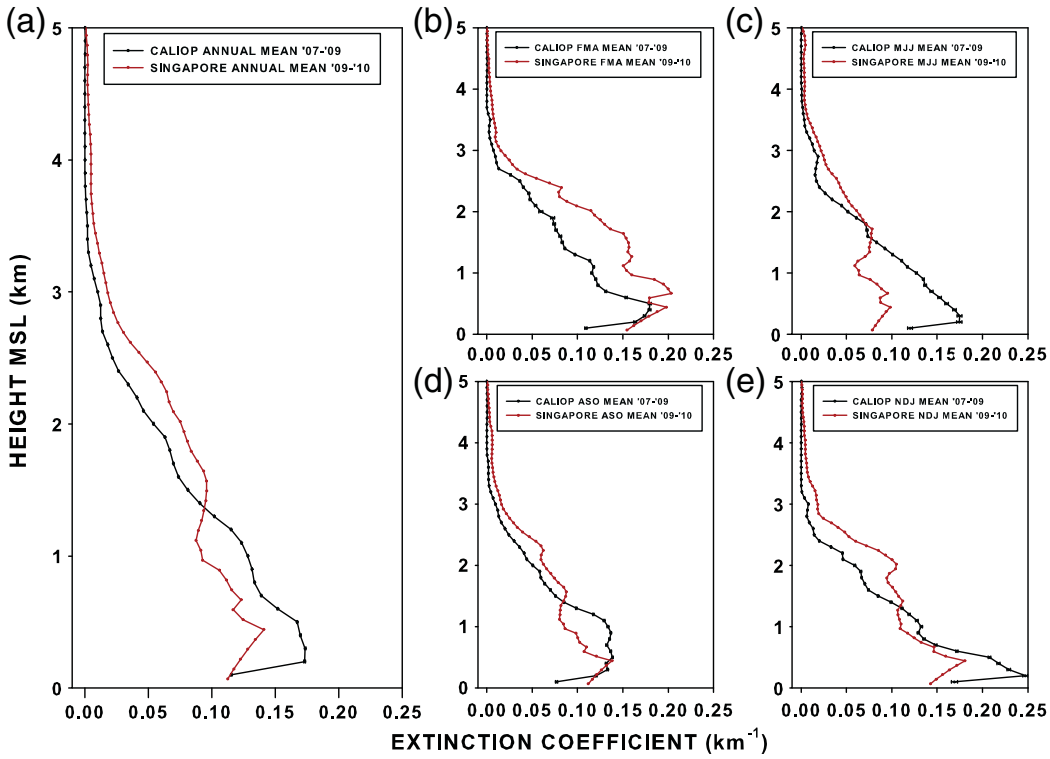

Fig. 16. For the Sumatra North sector (Fig. 4; Table 2; 100° E/14° N–104° E/20° N) (a) 2007–2009 mean annual 0.532 μm CALIOP extinction coefficient profile and mean November 2009–June 2011 Micropulse Lidar Network 0.527 μm extinction coefficient profile collected at Singapore (see inset; 1.30° N, 103.77° E, 79 m MSL), with corresponding seasonal averages for (b) FMA, (c) MJJ, (d) ASO and (e) NDJ.

represented near the surface in lieu of the "polluted continental" model contributing most to total extinction. Since both models are assigned 70 sr for lidar ratio, this finding is less significant. For reference, however, the mean annual MPLNET lidar ratio solved at Singapore was 48.0, which is in fact lower than the assigned lidar ratios for polluted continental, polluted dust and smoke, indicating that less absorptive marine aerosols, like sea salts, may be more prominent near this site.

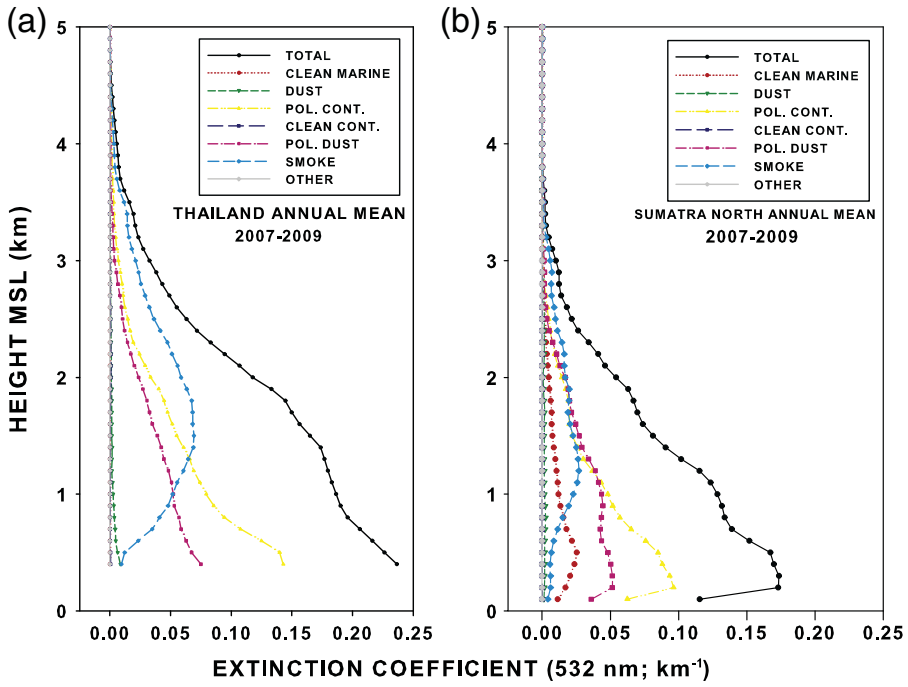

Fig. 17. Corresponding with Figs. 15a and 16a, for the mean annual 0.532 μm CALIOP extinction coefficient profile for the Thailand and Sumatra North sectors, respectively, the fractional contributions to total extinction for seven of the CALIOP aerosol types used for assigning the a-priori lidar ratio value used in the retrieval (see inset for titles).

The SN NDJ profile and the magnitude of the derived extinction coefficient vary from that seen in the regional CALIOP composites (Figs. 7–10). There, the highest and most persistent values are found corresponding with the season of maximum regional burning activity during ASO. The ASO profile from both CALIOP and MPLNET (Fig. 16d) instead exhibits a lower integrated AOD than in NDJ. When considered in light of relatively weak and shallow outflow from the islands northward into the South China Sea region during ASO, this may be the result of changes to preferential trajectories and/or the efficacy of cloud indirect scavenging of aerosol particles in this sector. Greater context for investigating this question is given in companion papers in this Special Issue (Salinas et al., 2013–this issue; Xian et al., 2013–this issue). However, this issue also requires a subsequent investigation.

5. Conclusions and impact

In this paper, a comprehensive assessment of the 0.532 μm vertical profile for aerosol particle extinction coefficient and linear depolarization, as well as aerosol composition and regional sources, are described from 2007 to 2009 over Southeast Asia and the surrounding waters and islands of the Maritime Continent (SA/MC). A quality-screened and cloud-cleared subset of Version 3.01 Level 2 NASA Cloud Aerosol Lidar with Orthogonal Polarization (CALIOP) 5-km Aerosol Profile datasets is studied. The *U.S. Naval Aerosol Analysis and Predictive System* (NAAPS) global transport model, featuring two-dimensional variational assimilation of NASA Moderate Resolution Imaging Spectroradiometer and Multi-angle Imaging SpectroRadiometer (MISR) quality-assured aerosol optical depth (AOD) datasets, combined with regional ground-based lidar measurements, serve as contextual background for assessing CALIOP retrieval quality, identifying regional biases and evaluating overall satellite representativeness. As part of the ongoing Seven South East Asia Studies (7SEAS) field campaign, these results contribute to a growing database of annual and inter-seasonal aerosol particle physical attributes, which will improve studies of regional radiative closure (Wang et al., 2007; Chung et al., 2010; Kuhlmann and Quass, 2010) and improve parameterizations for numerical models tasked with resolving particle presence and structure.

The primary conclusions of this study are as follows:

1. CALIOP AOD retrievals are high over land relative to NAAPS in SA, including the islands of the MC (0.412/0.312, respectively, over land for averages of all data points inclusive, and 0.310/0.235 for sample-normalized per-bin averages). However, CALIOP is relatively low compared to NAAPS over open waters (0.102/0.151 for all data points and 0.086/0.124 in a per-bin average, respectively, over ocean). Regional means, however, are very similar (0.180/0.193 for all data points and 0.155/0.159 when averaged per normalized bin), as the two effects counterbalance one another. These offsets, particularly over land, exceed the expected range of NAAPS uncertainty based on interpretation of the model versus MODIS/MISR and NASA Aerosol Robotic Network AOD measurements. A priori assignment of the lidar extinction-to-backscatter ratio ("lidar ratio"), necessary to initialize CALIOP retrieval algorithms, is the likeliest source of these discrepancies. Over land, NAAPS indicates more dust present than CALIOP composition models are resolving. Therefore, it is considered likely that the lidar ratio is biased high when applied for over-land retrievals, thus representing an anomalous contribution of relatively absorbing aerosol particle types. Over water, the opposite scenario is occurring. Less-absorbing particle types identified in CALIOP retrievals result in lower lidar ratios and an underestimate of extinction coefficient and subsequent column-integrated AOD.
2. Over the waters of MC, except the Bay of Bengal, CALIOP retrievals indicate that most aerosol particle presence (0.532 μm extinction coefficient $<0.05\ km^{-1}$) is capped near 1.5 km MSL. Over land, capping occurs below roughly 3.0 km MSL. Ground-based lidar observations at Singapore indicate a potentially larger contribution of elevated aerosol particle scattering than do CALIOP regional composites. However, the lidar dataset was collected during 2009–2011, and thus the comparison is not definitive. Persistent cloudiness over this portion MC (over 80% of available 5-km data points screened in QA processing) may limit the representativeness of CALIOP for climatological assessment. Elevated particle outflow over surrounding waters is limited. CALIOP depicts a shallow (<1.50 km MSL) layer of significant outflow into the South China Sea. Yet, this environment in convectively unstable, and buoyancy from surface combustion should contribute to lofting efficiencies that surpass this level. This finding is noteworthy.
3. Linear depolarization of CALIOP backscatter signals indicates that aerosol particles nearest the surface, at 0.50 and 1.50 km MSL, are mostly spherical. The lone exception occurs in the far west over India, where a greater contribution of aspherical matter (i.e., likely dust) is found. This finding indicates that urban industrial haze, sea salt droplets and fresh smoke are likely the most common aerosol particle types in the SA/MC boundary layer. Above this height, dust is seen with increasing frequency when aerosol particles are present, which as discussed above varies a great deal throughout the region. Stratification and decoupling of aerosol particle layers in SA/MC are apparent from these results, complicating characterization of column composition typically requisite for interpreting satellite-based measurements of aerosol properties.

Cloud-free profiling in the MC is difficult. 60–80% of the available CALIOP data for this study are rejected for cloud presence and signal attenuation limits. The potential biasing of scattered aerosol particle radiances below optically-thin clouds limits the effectiveness of all satellite-based retrievals. This paper is, therefore, written with the implicit understanding that overall representativeness of the SA/MC aerosol system is not guaranteed using CALIOP. Though the means described for screening the CALIOP archive may be partially responsible, this further justifies the role and necessity of ground-based measurements for continuing validation and contextual comparison with the satellite sensor. Continuing field collects and research conducted through 7SEAS, combined with the promise for aircraft-based and even more robust field observations associated with the pending 2012 NASA Southeast Asia Composition, Cloud, Climate Coupling Regional Study (SEAC^{4}RS), can look to these results as both a critical context and a starting point from which to further the understanding of scattering and radiative properties

associated with SA/MC aerosol particles. Furthermore, critical parameters necessary for replicating the regional aerosol system for numerical models, such as spatial and temporal autocorrelation lengths as one example, can be evaluated based on this 2007–2009 data subset.

Studies such as this one can also be considered for improving CALIOP algorithms and sub-regional characterizations, thus ultimately contributing to an optimized data archive for use long after the mission is complete. Instruments capable of high spectral resolution retrievals of cloud and aerosol particle scattering, and therefore a direct means for distinguishing particulate and molecular extinction coefficients, are increasingly replacing elastic-scattering instruments (e.g., Grund and Eloranta, 1991). The next generation of satellite-based atmospheric lidars will be predicated on such standard capabilities. However, these instruments require precise laser tuning and stability, and therefore incur significant costs. It is plausible that the community will continue operating elastic-scattering lidars in significant numbers for at least another decade, meaning that an enormous global archive of elastic-scattering measurements will be available for a generation of research. It is critical that these data be processed with the most accurate value-added retrieval schemes available, and why studies like this one can contribute appreciably to lidar monitoring activities overall.

In closing, one aspect of this work that will require follow-up study, particularly during the SEAC^{4}RS experiment, is the difference between effective particle extinction top heights found over land versus water. As discussed, the bulk of aerosol particle mass is confined to within 2.5 km MSL over the former, whereas it is distributed much lower over the latter. Though the mean profiles of particle extinction solved in this study surely suppress episodic events, it is likely in this tropical and convective climate that these layer top heights corresponding with significant thermodynamic boundaries, vary vertically as a function of incident surface heating and vapor pressures over relatively dry land versus ocean. Further, the relatively clean layers above these heights likely reflect cloud processing and scavenging of particle mass. The ramifications for cloud indirect effect studies, therefore, are potentially massive. If the overwhelming majority of aerosol particle mass is subject to wet deposition and scavenging, this region represents a near optimally efficient natural laboratory for studying aerosol/cloud interactions, their inherent radiative anomalies and effects on regional climate, in general.

Acknowledgments

This research was funded by the Office of Naval Research Code 35. Author JRC acknowledges the support of NASA Interagency Agreement NNG11HG12I on behalf of the Micropulse Lidar Network (MPLNET). MPLNET is operated with the support of the NASA Radiation Sciences Program. The authors thank Mark A. Vaughan at NASA Langley Research Center with his help interpreting the CALIOP Level 2.0 Aerosol Profile datasets. The group acknowledges the NASA AERONET program, their contributing principal investigators and staff for coordinating the coastal and inland sites used in this investigation.

Appendix A

Applying a numerical model for evaluating the CALIOP datasets requires some basic assessment of skill and potential biases/caveats. 2007–2009 mean annual and seasonal NAAPS 0.550 μm AODs corresponding with CALIOP data points in Fig. 1 are shown in Supplemental Fig. S5a–e. In Supplemental Fig. S6, ground validation of NAAPS 00-h analysis and 24-h forecast AOD versus regional/co-located NASA Aerosol Robotic Network 0.550 μm sun photometer measurements (Holben et al., 1998) at coastal (i.e., over water; Fig. S6a and c, respectively) and over land sites (Fig. S6b and d, respectively) are shown for 2007. In Supplemental Fig. S7, NAAPS (Fig. S7a) and corresponding quality-assured MODIS/MISR mean annual AOD (Fig. S7b), again only for 2007, are shown along with correlation coefficient (Fig. S7c), root mean square deviation (RMSD; Fig. S7d), and the relative ratio (Fig. S7e) between the two datasets and number of data points (Fig. S7f) at each $1^\circ \times 1^\circ$ grid point, for the model 00-h analysis. Corresponding comparisons of NAAPS with MODIS/MISR for the 24-h model forecast, are shown in Supplemental Fig. S8a–f.

Similar to that reported by Campbell et al. (2012), analysis of the results shown in Figs. S5–8 leads to the conclusion that the model exhibits reasonable stability for conducting comparisons with CALIOP in SA/MC, thus leading to an interpretation of retrieval performance. Model AOD distributions (Fig. S5a–e) compare qualitatively well with CALIOP (Fig. 1a–e), both annually and seasonally. At 00-h, NAAPS analyses compare equally well with those derived from MODIS/MISR (Fig. S7a–b). Correlation coefficients derived comparing NAAPS with AERONET measurements exceed 0.75 over both land and coastal sites (Fig. S6a–b). Corresponding absolute errors are 0.10 and 0.12, respectively. Correlation between NAAPS and MODIS/MISR exceeds 0.90 at nearly all points (Fig. S7c). RMSD is less than 0.10 over most of the region, though offsets exist between over-land and over-ocean grid points (Fig. S7d). Ratios of relative AOD (Fig. S7e) indicate that the model is biased low over most over-land regions compared with MODIS/MISR, though the comparison with AERONET indicates that this relationship is influenced most by high AOD cases (>0.60; Fig. S6b). Over water, the datasets are relatively consistent.

Performance degrades with the 24-h NAAPS forecast, though this effect is more pronounced over land than water. Again, and as described further by Campbell et al. (2012), the 24-h forecast is necessary for evaluating the skill of any nighttime comparisons between CALIOP and NAAPS. That is, since there is no assimilation of MODIS/MISR conducted at nighttime, and no ground-validation observations from AERONET in the dark sector of the model, a full 24-h cycle/assessment is necessary to interpret/interpolate model skill when pairing NAAPS nighttime AOD with CALIOP retrievals. Offsets exist within the CALIOP archive between night and day (Campbell et al., 2012). For the purposes of this study, however, and when considered relative to the 30–50% land/ocean AOD offsets described above, these differences ($<10\%$) are relatively small.

AOD distributions solved by NAAPS qualitatively match well with MODIS/MISR (Fig. S8a–b), though NAAPS is low relative to the satellites along the southwestern base of the Himalayas in northern India, central Thailand, Sumatra and

Java and southeastern China. NAAPS is relatively high over the eastern Indo-Gangetic Plain. Correlation coefficients derived comparing with AERONET hold relatively steady at 0.73 over coastal sites, but drop noticeably to 0.46 over land (Fig. S6c–d). Absolute error jumps between the two slightly to 0.12 over coastal sites, but increases to 0.17 over land. Noticeable NAAPS low biases are seen in these data, however, again though the effect is most pronounced for higher AOD cases. Compared with MODIS/MISR, correlation varies between 0.40 and 0.80 (Fig. S8c), similar to that found comparing with AERONET. RMSD increases regionally (Fig. S8d), but notably exceeds 0.25 stretching from along the Indo-Gangetic Plain eastward into southeastern China. This result is believed to be the combined effect of both lesser model advective skill, weaknesses exhibited by the passive satellite retrievals regions of complex terrain (Shi et al., 2011b), and further struggles over the accompanying bright surfaces endemic to portions of this area (e.g., Hsu et al., 2004). Ratios between forecast and MODIS/MISR retrievals (Fig. S8e) reflect the same low bias depicted in AERONET comparisons over the bulk of the SA/MC, with an area of high bias over the eastern Indo-Gangetic Plain, northern Myanmar and Thailand. Over the southwestern and northeastern waters, these ratios are near unity.

Appendix B. Supplementary data

Supplementary data to this article can be found online at http://dx.doi.org/10.1016/j.atmosres.2012.05.007.

References

Ackerman, J., 1998. The extinction-to-backscatter ratio of tropospheric aerosol: a numerical study. J. Atmos. Ocean. Technol. 15, 1043–1050.

Adachi, K., Freney, E.J., Buseck, P.R., 2011. Shapes of internally mixed hygroscopic aerosol particles after deliquescence, and their effect on light scattering. Geophys. Res. Lett. 38, L13804. http://dx.doi.org/10.1029/2011GL047540.

Anderson, T.L., Charlson, R.J., Schwartz, S.E., Knutti, R., Boucher, O., Rodhe, H., Heintzenberg, J., 2003a. Climate forcing by aerosols — a hazy picture. Science 300, 1103–1104.

Anderson, T.L., Charlson, R.J., Winker, D.M., Ogren, J.A., Holmén, K., 2003b. Mesoscale variations of tropospheric aerosols. J. Atmos. Sci. 60, 119–136.

Aoki, K., 2008. Aerosol and cloud optical properties by ground-based sky radiometer measurements. Proc. SPIE 7027. http://dx.doi.org/10.1117/12.822504.

Bridge, N.J., Buckingham, A.D., 1966. The polarization of laser light scattered by gases. Proc. Roy. Soc. Lond. A 295, 334–349.

Campbell, J.R., Hlavka, D.L., Welton, E.J., Flynn, C.J., Turner, D.D., Spinhirne, J.D., Scott, V.S., Hwang, I.H., 2002. Full-time, eye-safe cloud and aerosol lidar observation at atmospheric radiation measurement program sites: instruments and data analysis. J. Atmos. Oceanic Technol. 19, 431–442.

Campbell, J.R., Reid, J.S., Westphal, D.L., Zhang, J., Hyer, E.J., Welton, E.J., 2010. CALIOP aerosol subset processing for global aerosol transport model data assimilation. J. Sel. Topics Appl. Earth Observ. Remote Sens. 3, 203–214. http://dx.doi.org/10.1109/JSTARS.2010.2044868.

Campbell, J.R., Tackett, J.L., Reid, J.S., Zhang, J., Curtis, C.A., Hyer, E.J., Sessions, W.R., Westphal, D.L., Prospero, J.M., Welton, E.J., Omar, A.H., Vaughan, M.A., Winker, D.M., 2012. Evaluating nighttime CALIOP 0.532 μm aerosol optical depth and extinction coefficient retrievals. Atmos. Meas. Tech. Discuss. 5, 2747–2794. http://dx.doi.org/10.5194/amtd-5-2747-2012.

Chung, C.E., Ramanathan, V., Carmichael, G., Kulkarni, S., Tang, Y., Adhikary, B., Leung, L.R., Qian, Y., 2010. Anthropogenic aerosol radiative forcing in Asia derived from regional models with atmospheric and aerosol data assimilation. Atmos. Chem. Phys. 10, 6007–6024. http://dx.doi.org/10.5194/acp-10-6007-2010.

Chuvieco, E., Justice, C., 2008. NASA earth observation satellite missions for global change research. In: Chuvieco, E. (Ed.), Earth Observation of Global Change: The Role of Satellite Remote Sensing in Monitoring the Global Environment. Springer, New York, pp. 23–38.

Dey, S., Di Girolamo, L., 2011. A decade of change in aerosol properties over the Indian subcontinent. Geophys. Res. Lett. 38, L14811. http://dx.doi.org/10.1029/2011GL048153.

Diner, D.J., et al., 1998. Multiangle Imaging SpectroRadiometer (MISR) description and experiment overview. IEEE Trans. Geosci. Remote Sens. 36, 1072–1087.

El-Askary, H., Gautam, R., Singh, R.P., Kafatos, M., 2006. Dust storms diction over the Indo-Gangetic basin using multi sensor data. Adv. Space Res. 37, 728–733.

Fernald, F.G., 1984. Analysis of atmospheric lidar observations: Some comments. Appl. Opt. 23, 652–653.

Flynn, C.J., Mendoza, A., Zheng, Y., Mathur, S., 2007. Novel polarization-sensitive micropulse lidar measurement technique. Opt. Express 15, 2785–2790.

Gettelman, A., Forster, de F., 2002. A climatology of the tropical tropopause layer. J. Meteorol. Soc. Jpn. 80 (4B), 911–924 P.M.

Giglio, L., Csiszar, I., Justice, C.O., 2006. Global distribution and seasonality of active fires as observed with the Terra and Aqua Moderate Resolution Imaging Spectroradiometer (MODIS) sensors. J. Geophys. Res. 111, G02016. http://dx.doi.org/10.1029/2005JG000142.

Gimmestad, G.G., 2008. Reexamination of depolarization in lidar measurements. Appl. Opt. 47, 3795–3802.

Grund, C.J., Eloranta, E.W., 1991. The University of Wisconsin high spectral resolution lidar. Opt. Eng. 30, 6–12.

Holben, B.N., Eck, T.F., Slutsker, I., Tanré, D., Buis, J.P., Setzer, A., Vermote, E., Reagan, J.A., Kaufman, Y.J., Nakajima, T., Lavenu, F., Jankowiak, I., Smirnov, A., 1998. AERONET — a federated instrument network and data archive for aerosol characterization. Remote Sens. Environ. 66, 1–16.

Hsu, N.C., Herman, J.R., Tsay, S.C., 2003. Radiative impacts from biomass burning in the presence of clouds during boreal spring in southeast Asia. Geophys. Res. Lett. 30 (5), 1224. http://dx.doi.org/10.1029/2002GL016485.

Hsu, N.C., Tsay, S.C., King, M.D., Herman, J.R., 2004. Aerosol properties over bright-reflecting source regions. IEEE Trans. Geosci. Remote Sens. 47, 557–569.

Hunt, W.H., Winker, D.M., Vaughan, M.A., Powell, K.A., Lucker, P.L., Weimer, C., 2009. *CALIPSO* lidar description and performance assessment. J. Atmos. Ocean. Technol. 26, 1214–1228.

Hyer, E.J., Chew, B.N., 2010. Atmospheric transport model evaluation of an extreme smoke episode in Southeast Asia. Atmos. Environ. 44, 1422–1427. http://dx.doi.org/10.1016/j.atmosenv.2010.01.043.

Hyer, E.J., Reid, J.S., Zhang, J., 2011. An over-land aerosol optical depth data set for data assimilation by filtering, correction, and aggregation of MODIS Collection 5 optical depth retrievals. Atmos. Meas. Tech. 4, 379–408.

Hyer, E.J., Reid, J., Prins, E., Hoffman, J., Schmidt, C., Giglio, L., Different views of fire activity over Indonesia and Malaysia from polar and geostationary satellite observations. Atmos. Res.

Intergovernmental Panel on Climate Change, 2007. In: Solomon, S., Qin, D., Manning, M., Chen, Z., Marquis, M., Averyt, K.B., Tignor, M., Miller, H.L. (Eds.), Climate Change 2007: The Physical Science Basis. Contribution of Working Group I to the Fourth Assessment Report of the Intergovernmental Panel on Climate Change. Cambridge University Press, Cambridge and New York. 996 pps.

Kang, I.S., Ho, C.H., Lim, Y.K., Lau, K.M., 1999. Principal modes of climatological seasonal and intraseasonal variations of the Asian summer monsoon. Mon. Wea. Rev. 127, 322–340. http://dx.doi.org/10.1175/1520-0493(1999) 127.

Kaufman, Y.J., Tanré, D., Remer, L.A., Vermote, E.F., Chu, A., Holben, B.N., 1997a. Operational remote sensing of tropospheric aerosol over land from EOS Moderate Resolution Imaging Spectroradiometer. J. Geophys. Res. 102, 17,051–17,067.

Kaufman, Y.J., Tanré, D.H., Gordon, R., Nakajima, T., Lenoble, J., Frouin, R., Grassl, H., Herman, B.M., King, M.D., Teillet, P.M., 1997b. Passive remote sensing of tropospheric aerosol and atmospheric correction for the aerosol effect. J. Geophys. Res. 102, 16,815–16,830.

King, M.D., Kaufman, Y., Menzel, P., Tanré, D., 1992. Remote sensing of cloud, aerosol and water vapor properties from the moderate resolution imaging spectrometer (MODIS). IEEE Trans. Geosci. Remote Sens. 30, 2–27.

King, M.D., Kaufman, Y.J., Tanré, D., Nakajima, T., 1999. Remote sensing of tropospheric aerosols from space: past, present and future. Bull. Am. Meteorol. Soc. 80, 2229–2259.

Kittaka, C., Winker, D.M., Vaughan, M.A., Omar, A., Remer, L.A., 2011. Intercomparison of column aerosol optical depths from CALIPSO and MODIS-Aqua. Atmos. Meas. Tech. 4, 131–141. http://dx.doi.org/10.5194/amt-4-131-2011.

Kuhlmann, J., Quass, J., 2010. How can aerosols affect the Asian summer monsoon? Assessment during three consecutive pre-monsoon seasons from CALIPSO satellite data. Atmos. Chem. Phys. 10, 4673–4688. http://dx.doi.org/10.5194/acp-10-4673-2010.

Lau, K.M., et al., 2008. The joint aerosol-monsoon experiment: a new challenge for monsoon climate research. Bull. Am. Meteorol. Soc. 89, 369–383.

Lee, H.N., Igarashi, Y., Chiba, M., Aoyama, M., Hirose, K., Tanaka, T., 2006. Global model simulations of the transport of Asian and Sahara dust: total

deposition of dust mass in Japan. Water Air Soil Pollut. 169, 137–166. http://dx.doi.org/10.1007/s11270-006-1895-8.
Liu, Z., Vaughan, M.A., Winker, D.M., Hostetler, C.A., Poole, L.R., Hlavka, D., Hart, W., McGill, M., 2004. Use of probability distribution functions for discriminating between cloud and aerosol in lidar backscatter data. J. Geophys. Res. 109, D15202. http://dx.doi.org/10.1029/2004JD004732.
Liu, Z., Hunt, W., Vaughan, M., Hosteller, C., McGill, M., Powell, K., Winker, D., Hu, Y., 2006. Estimating random errors due to shot noise in backscatter lidar observations. Appl. Opt. 45, 4437–4447.
Liu, Z., et al., 2008. CALIPSO lidar observations of the optical properties of Saharan dust: a case study of long-range transport. J. Geophys. Res. 113, D07207. http://dx.doi.org/10.1029/2007JD008878.
Liu, Z., Vaughan, M., Winker, D., Kittaka, C., Getzewich, B., Kuehn, R., Omar, A., Powell, K., Trepte, C., Hostetler, C., 2009. The *CALIPSO* lidar cloud and aerosol discrimination: version 2 algorithm and initial assessment of performance. J. Atmos. Oceanic Technol. 26, 1198–1213.
Loeb, N.G., Wielicki, B.A., Doelling, D.R., Smith, G.L., Keyes, D.F., Kato, S., Manalo-Smith, N., Wong, T., 2009. Toward optimal closure of the earth's top-of-atmosphere radiation budget. J. Climate 22, 748–766. http://dx.doi.org/10.1175/2008JCLI2637.
Loeb, N.G., Manalo-Smith, N., Kato, S., Miller, W.F., Gupta, S.K., Minnis, P., Wielicki, B.A., 2003. Angular distribution models for top-of-atmosphere radiative flux estimation from the clouds and the earth's radiant energy system instrument on the Tropical Rainfall Measuring Mission Satellite. Part I: methodology. J. Appl. Meteor. 42, 240–265. http://dx.doi.org/10.1175/1520-0450(2003) 042.
Luo, G., Yu, F., Wang, A., 2009. Impact of aerosol on sea surface temperature over the subtropical Atlantic Ocean: a potential trigger factor of the NAO phase conversion? Geophys. Res. Lett. 36, L03708. http://dx.doi.org/10.1029/2008GL036035.
Martonchik, J.V., Diner, D.J., Kahn, R.A., Ackerman, T.P., Verstraete, M.M., Pinty, B., Gordon, H.R., 1997. Techniques for the retrieval of aerosol properties over land and ocean using multiangle imaging. IEEE Trans. Geosci. Remote Sens. 36, 1212–1227.
McFarquhar, G.M., Heymsfield, A.J., Spinhirne, J., Hart, B., 2000. Thin and subvisual tropopause tropical cirrus: observations and radiative impacts. J. Atmos. Sci. 12, 1841–1853.
Measures, R.M., 1984. Laser Remote Sensing: Fundamentals and Applications. Wiley. 510 pp.
Mishchenko, M.I., Hovenier, J.W., 1995. Depolarization of light backscattered by randomly oriented nonspherical particles. Opt. Lett. 20, 1356–1358.
Mischenko, M.I., Cairns, B., Kopp, G., Schueler, C.F., Faful, B.A., Hansen, J.E., Hooker, R.J., Itchkawich, T., Maring, H.B., Travis, L.D., 2007. Accurate monitoring of terrestrial aerosols and total solar irradiance. Bull. Amer. Meteorol. Soc. 88, 677–691.
National Aeronautics and Space Administration, 2010. Cloud–Aerosol LIDAR Infrared Pathfinder Satellite Observations (CALIPSO), Data Management System, Data Products Catalog. PC-SCI-503, Release 3.2. Langley Research Center, Hampton, Virginia. 84 pp.
Nishizawa, T., Sugimoto, N., 2009. Aerosol observation research using "LIDAR" active laser remote sensing instruments. Earozoru Kenkyu 24 (in Japanese).
Omar, A.H., Winker, D.M., Kittaka, C., Vaughan, M.A., Liu, Z., Hu, Y., Trepte, C.R., Rogers, R.R., Ferrare, R.A., Lee, K.P., Kuehn, R.E., Hostetler, C.A., 2009. The CALIPSO automated aerosol classification and lidar ratio selection algorithm. J. Atmos. Ocean. Technol. 26, 1994–2014.
Oo, M., Holz, R., 2011. Improving the CALIOP aerosol optical depth using combined MODIS-CALIOP observations and CALIOP integrated attenuated total color ratio. J. Geophys. Res. 116, D14201. http://dx.doi.org/10.1029/2010JD014894.
Reid, J.S., Hyer, E.J., Prins, E.M., Westphal, D.L., Zhang, J., Wang, J., Christopher, S.A., Curtis, C.A., Schmidt, C.C., Eleuterio, D.P., Richardson, K.A., Hoffman, J.P., 2009. Global monitoring and forecasting of biomass-burning smoke: description of and lessons from the Fire Locating and Modeling of Burning Emissions (FLAMBE) Program. IEEE J. Sel. Topics Appl. Earth Observ. Remote Sens. JSTARS-2009-00034.
Reid, J.S., Xian, P., Hyer, E.J., Flatau, M.K., Ramirez, E.M., Turk, F.J., Sampson, C.R., Zhang, C., Fukada, E.M., Maloney, E.D., 2012. Multi-scale meteorological conceptual model of observed active fire hotspot activity and smoke optical depth in the Maritime Continent. Atmos. Chem. Phys. 12, 2117–2147. www.atmos-chem-phys.net/12/2117/2012/doi:10.5194/acp-12-2117-2012.
Reid, J.S., Hyer, E.J., Johnson, R.S., Holben, B.N., Yokelson, R.J., Zhang, J., Campbell, J.R., Christopher, S.A., Di Girolamo, L., Giglio, L., Holz, R.E., Kearney, C., Miettinen, J., Reid, E.A., Turk, F.J., Wang, J., Xian, P., Zhao, G., Balasubramanian, R., Chew, B.N., Janjai, S., Lagrosas, N., Lestari, P., Lin, N.-H., Mahmud, M., Nguyen, A.X., Norris, B., Oanh, N.T.K., Oo, M., Salinas, S.V., Welton, E.J., Liew, S.C., 2013. Observing and understanding the Southeast Asian aerosol system by remote sensing: An initial review and analysis for the Seven Southeast Asian Studies (7SEAS) program. Atmos Res. 122, 403–468 (this-issue).
Remer, L.A., et al., 2005. The MODIS aerosol algorithm, products, and validation. J. Atmos. Sci. 62, 947–973.
Remer, L.A., et al., 2008. Global aerosol climatology from the MODIS satellite sensors. J. Geophys. Res. 113, D14S07. http://dx.doi.org/10.1029/2007JD009661.
Riihimaki, L.D., McFarlane, S.A., 2010. Frequency and morphology of tropical tropopause layer cirrus from CALIPSO observations: are isolated cirrus different from those connected to deep convection? J. Geophys. Res. 115, D18201. http://dx.doi.org/10.1029/2009JD013133.
Rotstayn, L.D., Penner, J.E., 2001. Indirect aerosol forcing, quasi forcing, and climate response. J. Climate 14, 2960–2975.
Salinas, S.V., Chew, B.N., Miettinen, J., Campbell, J.R., Welton, E.J., Reid, J.S., Yu, L.E., Liew, S.C., 2013. Physical and optical characteristics of the October 2010 haze event over Singapore: a photometric and lidar analysis. Atmos. Res. 122, 555–570 (this-issue).
Sassen, K., 1991. The polarization lidar technique for cloud research: a review and current assessment. Bull. Amer. Meteorol. Soc. 72, 1848–1866.
Sassen, K., 2000. Lidar backscatter depolarization technique for cloud and aerosol research. In: Mishchenko, M.I., Hovenier, J.W., Travis, L.D. (Eds.), Light Scattering by Nonspherical Particles: Theory, Measurements, and Applications. Academic Press, San Diego, pp. 393–417. Academic Press.
Sassen, K., 2005. Polarization in lidar. In: Wietkamp, C. (Ed.), Lidar: range-resolved optical remote sensing of the atmosphere. Springer, pp. 19–42.
Sassen, K., Cho, B.S., 1992. Subvisual-thin cirrus lidar dataset for satellite verification and climatological research. J. Appl. Meteor. 31, 1275–1285.
Sassen, K., Zhu, J., Webley, P., Dean, K., Cobb, P., 2007. Volcanic ash plume identification using polarization lidar: Augustine eruption, Alaska. Geophys. Res. Lett. 34, L08803. http://dx.doi.org/10.1029/2006GL027237.
Schotland, R.M., Sassen, K., Stone, R.J., 1971. Observations by lidar of linear depolarization ratios by hydrometeors. J. Appl. Meteor. 10, 1011–1017.
Schwartz, S.E., Andreae, M.O., 1996. Uncertainty in climate change caused by aerosols. Science 272, 1121.
Shi, Y., 2009. Development of data-assimilation-quality MODIS and MISR over water aerosol products, M. S. thesis, Department of Atmospheric Sciences, University of North Dakota, 74 pp.
Shi, Y., Zhang, J., Reid, J.S., Holben, B., Hyer, E.J., Curtis, C., 2011a. An analysis of the Collection 5 MODIS over-ocean aerosol optical depth product for its implication in aerosol assimilation. Atmos. Chem. Phys. 11, 557–565. http://dx.doi.org/10.5194/acp-11-557-2011.
Shi, Y., Zhang, J., Reid, J.S., Hyer, E.J., Eck, T.F., Holben, B.N., Kahn, R.A., 2011b. A critical examination of spatial biases between MODIS and MISR aerosol products - application for potential AERONET deployment. Atmos. Meas. Tech. 4, 2823–2836. http://dx.doi.org/10.5194/amt-4-2823-2011.
Shimizu, A., Sugimoto, N., Matsui, I., Arao, K., Uno, I., Murayama, T., Kagawa, N., Aoki, K., Uchiyama, A., Yamazaki, A., 2004. Continuous observations of Asian dust and other aerosols by polarization lidars in China and Japan during ACE-Asia. J. Geophys. Res. 109, D19S17. http://dx.doi.org/10.1029/2002JD003253.
Stephens, G.L., et al., 2002. The CloudSat mission and the A-Train. Bull. Amer. Meteorol. Soc. 83, 1771–1790. http://dx.doi.org/10.1175/BAMS-83-12-1771.
Tackett, J.L. and coauthors: Designing a level 3 aerosol optical property dataset for CALIPSO, manuscript in preparation.
Tanré, D., Kaufman, Y.J., Herman, M., Matto, S., 1997. Remote sensing of aerosol properties over oceans using the MODIS/EOS spectral radiance. J. Geophys. Res. 102, 16,971–16,988.
Tian, B., Waliser, D.E., Kahn, R.A., Li, Q., Yung, Y.L., Tyranowski, T., Geogdzhayev, I.V., Mishchenko, M.I., Torres, O., Smirnov, A., 2008. Does the Madden–Julian oscillation influence aerosol variability? J. Geophys. Res. 113, D12215. http://dx.doi.org/10.1029/2007JD009372.
Uno, I., Eguchi, K., Yumimoto, K., Takemura, T., Shimizu, A., Uematsu, M., Liu, Z., Wang, Z., Hara, Y., Sugimoto, N., 2009. Asian dust transported one full circuit around the globe. Nat. Geosci. 2, 557–560. http://dx.doi.org/10.1038/ngeo583.
Vaughan, M.A., Powell, K.A., Kuehn, R.E., Young, S.A., Winker, D.M., Hostetler, C.A., Hunt, W.H., Liu, Z., McGill, M.J., Getzewich, B.J., 2009. Fully automated detection of cloud and aerosol layers in the CALIPSO lidar measurements. J. Atmos. Ocean. Technol. 26, 2034–2050.
Virts, K.S., Wallace, J.M., 2010. Annual, interannual, and intraseasonal variability of tropical tropopause transition layer cirrus. J. Atmos. Sci. 67, 3097–3112.
Wang, S.H., Lin, N.H., Chou, M.D., Woo, J.H., 2007. Estimate of radiative forcing of Asian biomass-burning aerosols during the period of TRACE-P. J. Geophys. Res. 112, D10222. http://dx.doi.org/10.1029/2006JD007564.
Welton, E.J., Campbell, J.R., Spinhirne, J.D., Scott, V.S., 2001. Global monitoring of clouds and aerosols using a network of micro-pulse lidar systems. Proc. Int. Soc. Opt. Eng. 4153, 151–158.
Welton, E.J., Voss, K.J., Quinn, P.K., Flatau, P.J., Markowicz, K., Campbell, J.R., Spinhirne, J.D., Gordon, H.R., Johnson, J.E., 2002. Measurements of aerosol vertical profiles and optical properties during INDOEX 1999 using micro-pulse lidars. J. Geophys. Res. 107, 8019. http://dx.doi.org/10.1029/2000JD000038.
Winker, D.M., Vaughan, M., Hunt, W., 2006. The CALIPSO mission and initial results from CALIOP. Proc. SPIE 6409, 640902. http://dx.doi.org/10.1117/12.698003.

Winker, D.M., Vaughan, M.A., Omar, A., Hu, Y., Powell, K.A., Liu, Z., Hunt, W.H., Young, S.A., 2009. Overview of the CALIPSO mission and CALIOP data processing algorithms. J. Atmos. Ocean. Technol. 26, 2310–2323.
Winker, D.M., Pelon, J., Coakley Jr., J.A., Ackerman, S.A., Charlson, R.J., Colarco, P.R., Flamant, P., Fu, Q., Hoff, R., Kittaka, C., Kubar, T.L., LeTreut, H., McCormick, M.P., Megie, G., Poole, L., Powell, K., Trepte, C., Vaughan, M.A., Wielicki, B.A., 2010. The CALIPSO mission: a global 3D view of aerosols and clouds. Bull. Amer. Meteorol. Soc. 91, 1211–1229.
Xian, P., Reid, J.S., Atwood, S.A., Johnson, R., Hyer, E.J., Sessions, W., Westphal, D.L., 2013. Smoke aerosol transport patterns over the Maritime Continent. Atmos. Res. 122, 469–485 (this-issue).
Yorks, J.E., McGill, M., Rodier, S., Vaughan, M., Hu, Y., Hlavka, D., 2009. Radiative effects of African dust and smoke observed from Clouds and the Earth's Radiant Energy System (CERES) and Cloud–Aerosol Lidar with Orthogonal Polarization (CALIOP) data. J. Geophys. Res. 114, D00H04. http://dx.doi.org/10.1029/2009JD012000.
Young, S.A., Vaughan, M.A., 2009. The retrieval of profiles of particulate extinction from Cloud–Aerosol Lidar Infrared Pathfinder Satellite Observations (CALIPSO) data: algorithm description. J. Atmos. Ocean. Technol. 26, 1105–1119.
Zhang, J., Reid, J.S., 2006. MODIS aerosol product analysis for data assimilation: assessment of Level 2 aerosol optical thickness retrievals. J. Geophys. Res. 111, D22207. http://dx.doi.org/10.1029/2005JD006898.
Zhang, J., Reid, J.S., 2009. An analysis of clear sky and contextual biases using an operational over ocean MODIS aerosol product. Geophys. Res. Lett. 36, L15824. http://dx.doi.org/10.1029/2009GL038723.
Zhang, J., Reid, J.S., Holben, B.N., 2005. An analysis of potential cloud artifacts in MODIS over ocean aerosol optical thickness products. Geophys. Res. Lett. 32, L15803. http://dx.doi.org/10.1029/2005GL023254.
Zhang, J., Reid, J.S., Westphal, D.L., Baker, N.L., Hyer, E.J., 2008. A system for operational aerosol optical depth data assimilation over global oceans. J. Geophys. Res. 113, D10208. http://dx.doi.org/10.1029/2007JD009065.
Zhang, J., Reid, J.S., 2010. A decadal regional and global trend analysis of the aerosol optical depth using a data-assimilation grade over-water MODIS and Level 2 MISR aerosol products. Atmos. Chem. Phys. 10, 10,949–10,963.
Zhang, J., Campbell, J.R., Reid, J.S., Westphal, D.L., Baker, N.L., Campbell, W.F., Hyer, E.J., 2011. Evaluating the impact of assimilating CALIOP-derived aerosol extinction profiles on a global mass transport model. Geophys. Res. Lett. 38, L14801. http://dx.doi.org/10.1029/2011GL047737.

Dr. James R. Campbell is a Meteorologist assigned to the Aerosol and Radiation Section at the Naval Research Laboratory in Monterey, CA. He received a Ph.D. in Atmospheric Sciences from the University of Alaska Fairbanks in 2006. He received B.S. and M.S. degrees in Meteorology from the University of Utah in 1993 and 1997, respectively. Dr. Campbell's scientific experience and research interests are in atmospheric remote sensing, aerosol and cloud physics and polar meteorology. The primary focus of his work is the characterization of aerosol and cloud physical properties using lidar (light detection and ranging) instruments.

Mr. Jason L. Tackett is an analyst for the CALIPSO Lidar Science Working Group at NASA Langley Research Center in Hampton, VA through Science Systems and Applications, Inc. He received an M.S. in Atmospheric Sciences from the University of Illinois at Urbana-Champaign in 2009 and a B.S in Physics from Kansas State University in 2007. His research interests include aerosol–cloud interactions, Saharan dust transport and aerosol optical property retrieval methods using lidar.